

Bucknell University

Bucknell Digital Commons

Master's Theses

Student Theses

Spring 2023

Characterizing Variability in the Transient Storage Zones of Miller Run in Lewisburg, PA

Sabrina Savidge
sms076@bucknell.edu

Follow this and additional works at: https://digitalcommons.bucknell.edu/masters_theses



Part of the [Civil and Environmental Engineering Commons](#)

Recommended Citation

Savidge, Sabrina, "Characterizing Variability in the Transient Storage Zones of Miller Run in Lewisburg, PA" (2023). *Master's Theses*. 264.

https://digitalcommons.bucknell.edu/masters_theses/264

This Masters Thesis is brought to you for free and open access by the Student Theses at Bucknell Digital Commons. It has been accepted for inclusion in Master's Theses by an authorized administrator of Bucknell Digital Commons. For more information, please contact dcadmin@bucknell.edu.

I, Sabrina M. Savidge, do grant permission for my thesis to be copied.

CHARACTERIZING VARIABILITY IN THE TRANSIENT STORAGE ZONES OF
MILLER RUN IN LEWISBURG, PA


by

Sabrina Savidge
sms076@bucknell.edu
Civil & Environmental Engineering
Bucknell University

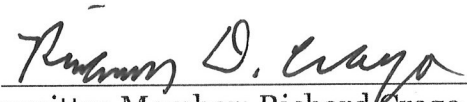
A Master's Thesis

Presented to the Faculty of
Bucknell University
In Partial Fulfillment of the Requirements for the Degree of
Master of Science in Civil & Environmental Engineering

Approved:


Adviser: Jessica Newlin, Ph.D.


Department Chairperson: Michael Malusis, Ph.D.


Thesis Committee Member: Richard Crago, Ph.D.


Thesis Committee Member: Matthew Higgins, Ph.D.

4/2023
(Date: Month and Year)

Acknowledgements

Thank you, Professor Jessica Newlin for providing me with the opportunity to work on this project and for helping me every step of the way through these two years. You have helped me so much and I appreciate everything that you have done to help me complete this project and thesis. I would also like to thank Professors Richard Crago and Matthew Higgins for being part of my committee. Their suggestions during the preparation of the project were helpful.

Additionally, thank you to Monica Hoover, Director of the Environmental and Science Lab, for allowing me to use the ion chromatography instrument to process data and for helping me with general troubleshooting. As well as Professor Rob Jacob, Geology & Environmental Geosciences, for his guidance on geophysical design, access to equipment, and technical help.

I would also like to thank my family, significant other, and friends for their encouragement and support during the completion of this thesis.

Table of Contents

Acknowledgements	iv
List of Tables	vi
List of Figures	vii
Terminology	ix
Notation	x
Abstract	xi
Introduction	1
Background	2
Groundwater and Surface Water Interaction	2
Transient Storage Zones	4
The Hyporheic Zone	7
Land Use Influence on Transient Storage Zones	8
Water Quality	9
Conservative Tracers and Transient Storage Models	11
Objective	14
Location and Site History	15
Methods	19
Site Investigation	20
Geophysical Methods	20
Tracer Studies and Modeling	25
OTIS Modeling	28
Results and Discussion	34
Site Investigation	34
Site A	37
Site B	41
Site C	45
Geophysics	48
Tracer Studies	57
Modeling Results	67
B2 Transient Storage Zone Modeling	68
B1 Transient Storage Zone Modeling	76
Conclusions	78
Tracer Study and Modeling Results	79
Geophysical Methods for Understanding Subsurface TSZs	80
Combining Tracer Study and Geophysical Data Findings	81
Bibliography	82
Appendix A - Matlab Code to Run OTIS-2Stor and Plot Results	87
Appendix B - OTIS-2Stor Input and Output Files for B2 Tracer Study	91
Appendix C - OTIS-2Stor Input and Output Files for B1 Tracer Study	94

List of Tables

Table 1.) Storage Zone Types and Resident Times	6
Table 2.) Materials and Availability	54
Table 3.) OTIS Parameters	76

List of Figures

Figure 1.) Multiple Storage Zones in a Theoretical Channel	5
Figure 2.) Curves Based on Injection Types	12
Figure 3.) Mass Balance Components in a Channel Reach	14
Figure 4.) Aerial Overview of Miller Run	16
Figure 5.) Highlighted Watershed Area of Miller Run	18
Figure 6.) Highlighted Stream Sections of Proposed Study Sites	19
Figure 7.) Electrode Grid for Electrical Resistivity	22
Figure 8.) Simple Electrical Resistivity Setup	23
Figure 9.) GPR Equipment	25
Figure 10.) Example Tracer Injection and Sampling Site of Tracer Test	26
Figure 11.) Two Breakthrough Curves From Tracer	29
Figure 12.) Soil Overview of Area	35
Figure 13.) Riparian Buffer Map	36
Figure 14.) Photo of Split Channel at Site A	37
Figure 15.) Pool at Site A	38
Figure 16.) Restored Gement in Site A	39
Figure 17.) Land Cover Types of Site A	40
Figure 18.) Riffles at Site B	42
Figure 19.) Transient Storage Zones in Site B	43
Figure 20.) Upstream View of Incised Channel	44
Figure 21.) Percent Land Coverage Types at Site B	45
Figure 22.) Dry Bed and Vegetation of Site C	46
Figure 23.) Low Flow at Site C	47
Figure 24.) Land Cover Present at Site C	48
Figure 25.) Initial GPR Radargram	49
Figure 26.) Radargram of Site C with Potential Tree	50
Figure 27.) GPR with Possible Second Interface	51
Figure 28.) Radargram without Details	51
Figure 29.) Apparent Resistivity Crossplots	53
Figure 30.) Different Views of Inverted Image	55
Figure 31.) Visual of Resistivity Results from Site B	56
Figure 32.) B1 Tracer Injection and Sampling Locations	59
Figure 33.) Mini Well Lengths	60
Figure 34.) Closeup of Mini Well Opening	60
Figure 35.) Flow Conditions During B1	61
Figure 36.) B1 Tracer Results	63

Figure 37.) Closeup of Flow Conditions During B2	64
Figure 38.) Portion of Tracer Setup	66
Figure 39.) B2 Tracer Results	67
Figure 40.) Site 1 OTIS-2Stor Simulation	70
Figure 41.) Site 3 OTIS-2Stor Simulation	71
Figure 42.) Site 4 OTIS-2Stor Simulation	72
Figure 43.) Site 5 OTIS-2Stor Simulation	73
Figure 44.) Storage Zone Results Using OTIS-2Stor	74
Figure 45.) Attempted B1 Model	78

Terminology

Continuous-Injection Tracer Test - A tracer injection method where a nonreactive solute is injected at a constant rate and measured at locations downstream at regular time intervals.

Electrical Resistivity (ER) - A geophysical method that involves applying an electrical current into a medium using an array of electrodes, and the potential difference between materials provides information of subsurface conditions.

Ground Penetrating Radar (GPR) - A method that uses electromagnetic frequencies and the resulting travel time between antennas to receive reflected pulses. The time it takes for a reflection to be received is dependent on the velocities of the material. It can detect material changes and buried objects.

Groundwater (GW) - Water that fills interstitial space within the subsurface.

Hyporheic Zone (HZ) - Intermediate areas between groundwater and surface water that receive through flow from both groundwater and surface water. In stream channels, downstream surface water flow exchanges regularly with the HZ on its path.

One-Dimensional Transport with Inflow and Storage (OTIS) - A free modeling software provided by the USGS that is a mathematical simulation model for advection and dispersion processes in surface water with lateral inflow and exchange with storage areas.

Surface Water (SW) - Water that exists in a surface water body i.e., lake, stream, wetland, sea.

Transient Storage Zone (TSZ) - Slow moving areas within surface water or stream beds that stagnant water flow.

Transient Storage Model (TSM) - A model that is commonly used in the analysis of surface water and groundwater exchanges.

Notation

C - main flow zone solute concentration [M/L³]

Q - volumetric flow rate [L³/T]

A - main flow cross-sectional area [L²]

D - dispersion coefficient [L²/T]

q_{Lin} - lateral inflow rate [L³/T-L]

C_L - lateral inflow solute concentration [M/L³]

L_{in} - lateral inflow solute concentration [M/L³]

α_1 - storage zone 1 exchange coefficient [/T]

C_{S1} - storage zone 1 solute concentration [M/L³]

α_2 - storage zone 2 exchange coefficient [/T]

C_{S2} - storage zone 2 solute concentration [M/L³]

A_{S1} - storage zone 1 cross-sectional area [L²]

A_{S2} - storage zone 2 cross-sectional area [L²]

t_{stor} - residence time of storage zone [T]

t - time [T]

x - distance [L]

L - unit of length

T - unit of time

M - unit of mass

Abstract

The transient storage zone processes are investigated in a small second order stream with a 2.2 square kilometer watershed. The presence of transient storage zones in small streams impacts the available flow paths for water and results in a wider range of residence times for water and dissolved chemicals than would be predicted by considering only the main channel flow path. Residence times can be used to quantify the health of a stream as several biogeochemical and ecological processes occur in water slowed by transient storage.

Sections of the studied stream are impacted by varying types of stream restoration practices and watershed management practices. These practices lead to the presence of a wide range of transient storage zone types. A combination of data collection, field experimentation, and data analysis is used to characterize the variability in transient storage zone processes and residence times in the small stream and to relate the identified storage zone processes to physical characteristics of the stream.

Field experimentation took place along measured sections and included geophysical investigations of the subsurface and continuous-injection tracer studies using a conservative tracer with sampling from the main channel flow and from identified transient storage zones following the continuous injection of tracer. Data analysis leads to a preliminary understanding of how various stream and watershed management practices can impact the presence of transient storage zones and the range of residence times and flow paths in small streams.

Introduction

Management of freshwater supply and water quality traditionally focused on one component of the water cycle, but the interconnected nature of the hydrologic system requires larger-scale management practices. Only 2.5 percent of the total global water is considered to be freshwater. Which includes surface water, groundwater, and freshwater trapped within glaciers. Only 1.2 percent of the total freshwater present on Earth is easily accessible surface water for consumption and groundwater makes up roughly 30 percent of the total freshwater (U.S. Geological Survey, 2021). Rivers and lakes contain a total of 92950.5 km³ of water worldwide, but these are the primary source of water for most people (U.S. Geological Survey, 2021). Surface water management regarding quantity and quality of water must consider the management of groundwater as well.

Groundwater aquifers, water bodies in the subsurface that are fully saturated, get recharged by infiltrating precipitation, and can be easily contaminated.

Statistically, 22 percent of groundwater samples throughout the United States contain at least one contaminant at a level high enough to negatively affect human health (U.S. Geological Survey, 2021). Near surface aquifers can be polluted from in situ geologic materials, surface water sources, and from anthropogenic activity. Anthropogenic land use categories such as agriculture, commercial, residential, and industry all release contaminants that can run off the landscape during rain events and seep into underlying sediment to be carried far from the source by the natural movement of water (U.S. Geological Survey,

2021). Because of their connection, combined groundwater and surface water monitoring can be used to track and trace pollutant movement.

Background

Groundwater and Surface Water Interaction

Surface water is connected to groundwater in multiple physiographic landscapes (Winter et al., 1998). Groundwater flows along paths from recharge zones to discharge at the surface into bodies of water. These bodies of water include streams, lakes, and wetlands. Streams are able to gain water from groundwater inflow, recharge the groundwater beneath, or alternatively gain and recharge depending on the location within the reach (Winter et al., 1998).

Gaining streams are streams that get inflow from the surrounding saturated zone. Streams that lose water to the underlying sediment are called losing streams or disconnected streams. The water table will experience a raised bump beneath a disconnected stream that has a noticeable detachment between the streambed and the water table. Activity in the saturated zone does not affect the surface water in places with a disconnection from the groundwater system by the unsaturated zone.

The classification of a stream as gaining, losing, or disconnected is not constant in space or time. For example, gaining streams can also experience bank storage when stream level raises significantly enough during flooding events that water

enters the streambanks. Bank storage can be large enough that the water stored in the banks reduces the risk of flooding. As the flood stage rises, the water from the channel flows into the subsurface of the streambanks, resulting in a losing stream instead of the usual recharge pattern. As the flood stage falls, the water stored in the banks is released back into the channel creating a gaining stream. Other changes in local hydrologic patterns can reverse these classifications as well, and local anthropogenic practices such as groundwater pumping can also reverse the regular recharge pattern.

In addition to contributing to flood event discharges, natural elements within the underlying bed geomorphology are a control on flow velocity changes. Locations with an abrupt slope change or a meander where water direction changes promote recharge and discharge in the reach. Riffles are linked with groundwater recharge and deeper pools often cause upward seepage through the streambed (Winter et al., 1998).

The travel times of flow paths between surface water and groundwater range from days to millenia depending on the length of a given flowpath (Alley et al., 1999). Paths in local flow systems directly under the subsurface can quickly discharge into a neighboring body of water, as they are relatively shallow (ex. minutes, days, months). Deeper flow paths can carry water farther away from the point of infiltration at a regional scale (ex. years, centuries, millenia). For example, modeling of tritium considering surface water and groundwater exchange in the Florida Everglades yielded an average residence time of

approximately 90 years (Harvey et al. 2006). The longer water spends underground, the opportunity for compositional changes increase. However, shorter, shallower flow paths are more sensitive to contamination from the surface.

Regular exchanges of water with different surface and subsurface characteristics leads to the evolution of the chemical makeup of water as it flows through different biological communities and sediments. Pollutants in either the surface or subsurface can potentially travel large distances from their origin because of this ongoing interchange.

Transient Storage Zones

The transient storage zone (TSZ) refers to areas in a stream channel where water enters pockets of slower velocity water or enters porous material in the streambed (Runkel, 2000). The TSZ promotes mixing of water and increases residence time of water in hydrologic systems. Surficial storage areas exist in vegetated areas, cavities, and obstacles that alter the flow pattern (Noh et al., 2021). Vegetation and bedforms make up a large portion of transient storage zones. Areas on large sediment deposits, such as point bars, interrupt the normal flow patterns, reducing velocities of water and trapping water in vortices. Obstacles, submerged or emergent, also cause delays in circulation and diverted flow. A graphical sketch of these different types of TSZs is shown in Figure 1.

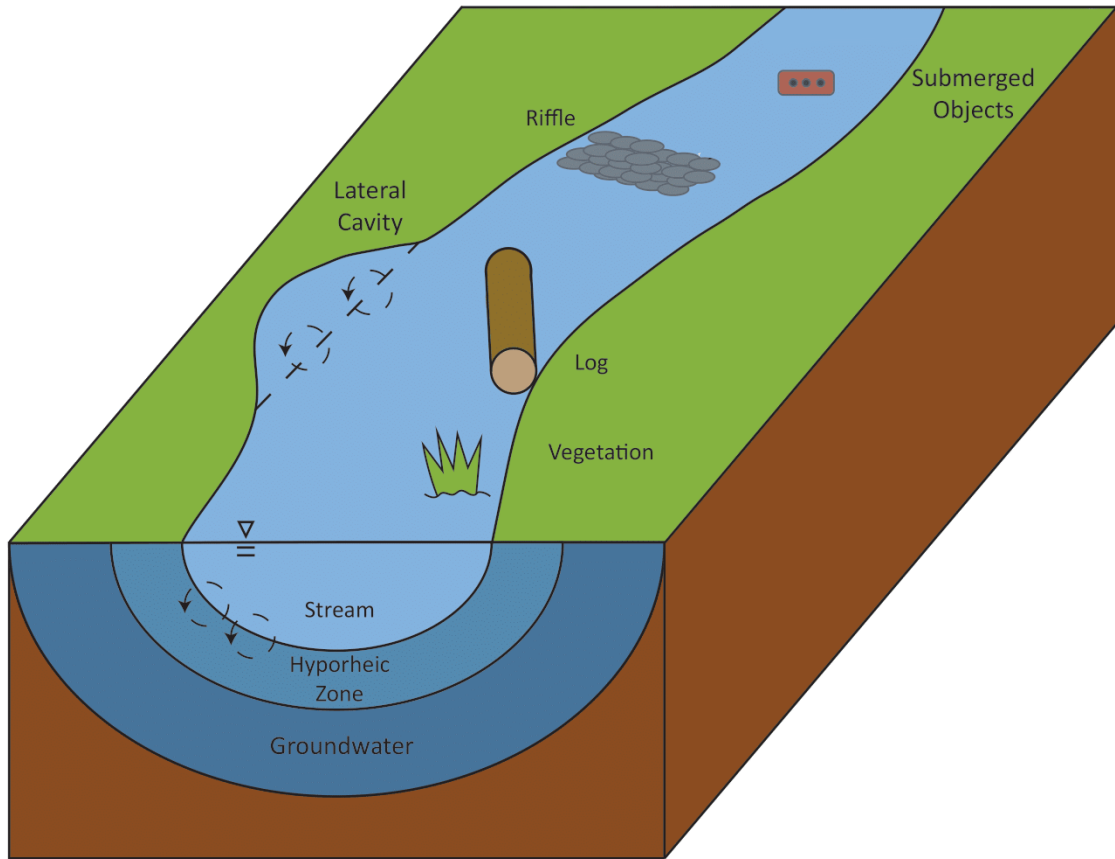


Figure 1.) Multiple storage zones are illustrated on the surface of a representational stream channel. The simplified schematic was developed based on Noh et al. (2021).

A specific type of TSZ is the hyporheic zone (HZ) that is made up of the pore spaces in the streambed and bank sediments. Figure 1 also shows the HZ as one of the multiple storage areas that can be present in an alluvial valley stream, and how it extends a depth from the wetted perimeter of a stream. Depending on stream characteristics, the HZ can vary widely in its size.

Modeling storage zone residence times by considering the interactions of surface water flow and transient storage zones becomes essential to understanding the behavior and travel of exchanging water in a stream. Due to the potential presence of multiple TSZs, including the HZ, there will be multiple surface water flow paths exchanging with these slower moving zones at different rates. This is similar to the range of residence times that can be observed with larger-scale surface water and groundwater interactions. Residence times in TSZ (including the HZ) tend to be on the order of minutes to days (Table 1).

Table 1. Storage zone types from previous tracer studies.

Storage Zone Type	Example	Hydrologic Residence Time	References
Periphyton-colonized films on streambed	Little Lost Man Creek, CA	3 min	Kim et al. (1990)
Aquatic vegetation zone at channel sides	Pinal Creek, AZ	4 – 35 min	Choi (1998)
Wetland floating vegetation	Everglades National Park, FL	54 min	Harvey et al. (2005)
Streambed sediments	St. Kevin Gulch, CO Pinal Creek, AZ Little Lost Man Creek, CA	6 hrs 1 – 25 min 6 – 25 hrs	Harvey et al. (1996) Harvey and Fuller (1998) Triska et al. (1993)
Wetland flocculent material and shallow peat	Everglades National Park, FL	20 hr	Harvey et al. (2005)
Alluvial sediments (greater than 5 m from stream)	North Fork Dry Run, VA Little Lost Man Creek, CA Aspen Creek and Rio Calaveras, NM	6 days 5 – 19 days 10 days	Castro et al. (1991) Triska et al. (1993) Wroblicky et al. (1998)
Lateral Cavities	Elder Creek, CA Oak Creek, OR Soap Creek, OR	8.9 min 6 - 10 min 5 - 29 min	O'Connor et al. (2010) Jackson et al. (2012) Jackson et al. (2012)

The Hyporheic Zone

The hyporheic zone (HZ) is a specific type of TSZ and is an ecotone or a transitional region between two biological communities in which surface water passes through along its flow path, and can vary in thickness, including more than 1000 m from the surface water channel (Chen, 2011). In streams and rivers, this zone connects surface flow and shallow subsurface flow regions and therefore serves as an important interface between surface and groundwater environments. Water that enters the HZ experiences a delay prior to dissemination along flow paths if the velocity of the flow paths is much slower than the overlying surface water body (Zarnetske et al., 2011). These differences can be seen in Table 1 where alluvial sediments have multi-day hydrologic residence times while aquatic vegetation zones and natural lateral cavities have residence times of several minutes.

Many processes exist within the HZ, including chemical reactions, solute and particle transport, temperature exchange, and microbial activity (Wondzell, 2011). The microorganisms that dominate the HZ are capable of decomposing organic material into nutrients, promoting sorption of metals, and biogeological weathering of surrounding sediments (Wondzell, 2011). These processes are ecosystem services that improve water quality. Multiple characteristics of the sediment and environment (including porosity, permeability, soil particle size, chemical features of the surface water body and groundwater, and physical

features of the stream itself) act as controls on these processes (Boano et al., 2014).

Land Use Influence on Transient Storage Zones

Different scales of land use change can influence the hydrologic processes in a stream system, including changes in runoff, changes in groundwater quality and quantity, types of TSZ that are present, and the flow paths connecting all of these features. Gooseff et al. (2007) examined six streams in urban, agricultural, and natural stream reaches to further investigate the potential impact that land use may have on transient storage. Streams that had experienced anthropogenic use possessed shorter residence times than the natural streams used for background comparison due to channelization and manipulation . These shorter residence times reduce the amount of biogeochemical cycling in the TSZ (Gooseff et al., 2007).

Riparian zones are land areas on either side of a stream that are usually covered with water loving vegetation and that function as the transition zone of river and terrestrial systems (Yochum, 2018). Practices of logging and clear cutting for agricultural purposes can minimize riparian zones. These riverside areas are in contact with surrounding landscape, surface water, and groundwater, and therefore they are connected to the HZ (Hester & Fox, 2020). The restoration or protection of riparian areas are often important elements in stream restoration efforts. However, quantifying their role in hydrologic processes of a stream channel has been difficult.

Characteristics that promote preferential flow paths such as paleochannels and gravel veins, underlie riparian zones (Hester and Fox, 2020). These preferential flow paths act as faster flow paths for groundwater, and can bypass processes that would otherwise occur in a TSZ. Essentially, these areas may expedite water that would otherwise linger in a TSZ for a longer amount of time. However, Herrman et al. (2010) found that riparian zones in headwater streams contribute less effect to storage residence times than macrophytes and flora such as cattails. Cattails are vegetation that is considered a surface transient storage zone. Additionally, the slower residence times caused by surface TSZs could contribute to increased surface water exchange with the HZ as well.

Water Quality

The chemical makeup of groundwater is greatly influenced by human activity, including land use changes. Conductivity values, pH, alkalinity, metal concentrations, among other characteristics have been linked to land use (Piscart et al., 2011). Agricultural practices and urbanization lead to several water quality concerns in surface water and groundwater systems.

In agricultural land particularly, nutrients from fertilizers and pesticides will get washed into surface water and groundwater systems during precipitation events. Similarly, animal waste will eventually percolate into the water table given enough time and lack of preventative measures. Concentrations of metals and fecal matter values have been observed to vary with seasonality (Brenner et al.,

1996). This phenomena may be linked with growing seasons, with the highest concentrations recorded in summer months. Peaks align with the growing and harvest season for several crops. Fecal coliform concentrations were higher in gaining streams receiving discharge by surrounding groundwater (Brenner et al., 1996). Septic drainage from adjacent lots and in situ sewage systems had higher counts than other non-agricultural land (Brenner et al., 1996). Fecal coliforms get carried through a watershed from the point of origin by groundwater and surface water exchanges, however, as it gets carried throughout the stream and surrounding streambed material it can be diluted.

Urbanization removes infiltration areas but also necessitates the need for management of infrastructure. Increases in cations, anions, and pH can be connected to urban areas. Runoff on impervious surfaces pick up contaminants from these surfaces and transport them into the surface water. In addition, towns, campuses, and the Department of Transportation use salts during winter months to maintain roadway infrastructure and prevent the formation of ice and enhance snowmelt. Eventually, these contaminants also wash into the surface water and groundwater systems.

Understanding the various residence times attributed to different flow paths and exchange between surface water and groundwater or surface water and TSZs becomes important for understanding the duration that contaminants may be present in hydrologic systems. The connected nature of groundwater and surface water means that water quality can be changed from the introduction of

contaminants that are carried downstream. Ions commonly linked to agriculture include but are not limited to nitrate, phosphates, and chlorides (Oenema et al., 2005). Understanding the transport of nutrients draining from agricultural land into channelized streams with less complex TSZs in the upper Mississippi River watershed has been undertaken to address the hypoxia in the Gulf of Mexico (Böhlke et al., 2009). More than half of the total nitrate load of a stream can be carried through riparian preferential flow zones and water infiltration is greatly increased in storm events (Hester and Fox, 2020).

Conservative Tracers and Transient Storage Models

Tracer studies can be used for characterizing transient storage zones, flow paths, residence times, and input and outputs in different hydrologic systems (Bruckner, 2021). Several kinds of tracers exist, including salts, dyes, and stable isotopes, that are widely used in watershed research (Bruckner, 2021). Reactive tracers (e.g. fluorescein) are able to undergo a prescribed chemical reaction once introduced to the stream, but conservative solute tracers (e.g. bromide) remain in a single phase when injected, and are non-reactive to surrounding chemical interactions (Shook et al., 2004).

Continuous-injection is a method of tracer injection that involves injecting a solute at a constant rate for a sufficiently long period that would create a plateau on the concentration-time curve at a downstream sampling location (Rantz, 1982). Rantz defined slug-injection (termed sudden-injection in the publication) as the instantaneous injection of tracer to a stream. Sampling downstream of the

injection will create a concentration-time curve that lacks a plateau. Figure 2 includes a comparison of the concentration-time curves that result from these two injection types (Rantz, 1982).

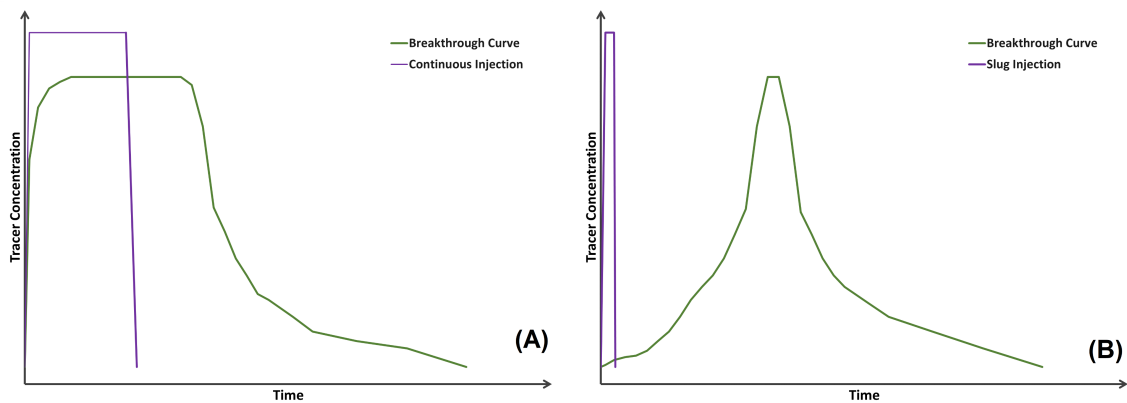


Figure 2.) The different curves that result from continuous-injection (A) and slug-injection (B) from Rantz (1982) showing the plateau vs peak that occur by each injection type.

Wright and Moore (2003) used both continuous-injection tests and slug-injections tests during their research project at a mine site in Southwestern Colorado. A combination of continuous-injection tests (LiBr) and a slug-injection test (NaCl), the solution poured into the stream at a slow rate over an hour instead of a standard instant application, were used to estimate discharge and any hydrologic connections between the stream and surrounding mines.

In another study using tracers, Sobota et al. (2012) used stable isotope tracers to separate organic matter storage from NO_3^- that was used in denitrification. They chose to use a continuous-injection method for the purpose of calculating discharge, water retention time, and specific discharge. Using the data, uptake

length (the distance traveled by the nitrate before reaching the surface), velocity, and the rate of denitrification in the stream sections were able to be derived. They were able to determine that land use did not have a significant effect on the nitrogen uptake rate and that NO_3^- used in denitrification was successfully separated out from the total uptake rate.

Conservative tracer studies have been used to study flow paths within HZ with the aid of transient storage models (TSM) that use complex exchanges that are sensitive to all exchange processes and solute storage effects not necessarily directly attributed to hyporheic flow (Packman and Bencala, 2000). One TSM model, the Solute Transport in Rivers (STIR) model, assumes conservation of mass for the tracer solute, where the mass introduced in the form of a tracer will then be accounted for at a downstream “exit” (Boano, 2014). Figure 3 is an example of the assumed mass balance equation where the total input (Q_{in}) must equal the output (Q_{out}) despite the exchanges occurring along the stream length (Q_{cav} and Q_{lat} exchanges). However, it is important to note that a TSM is not exclusively sensitive to hyporheic exchange and can register storage caused by a number of surficial storage zones as well.

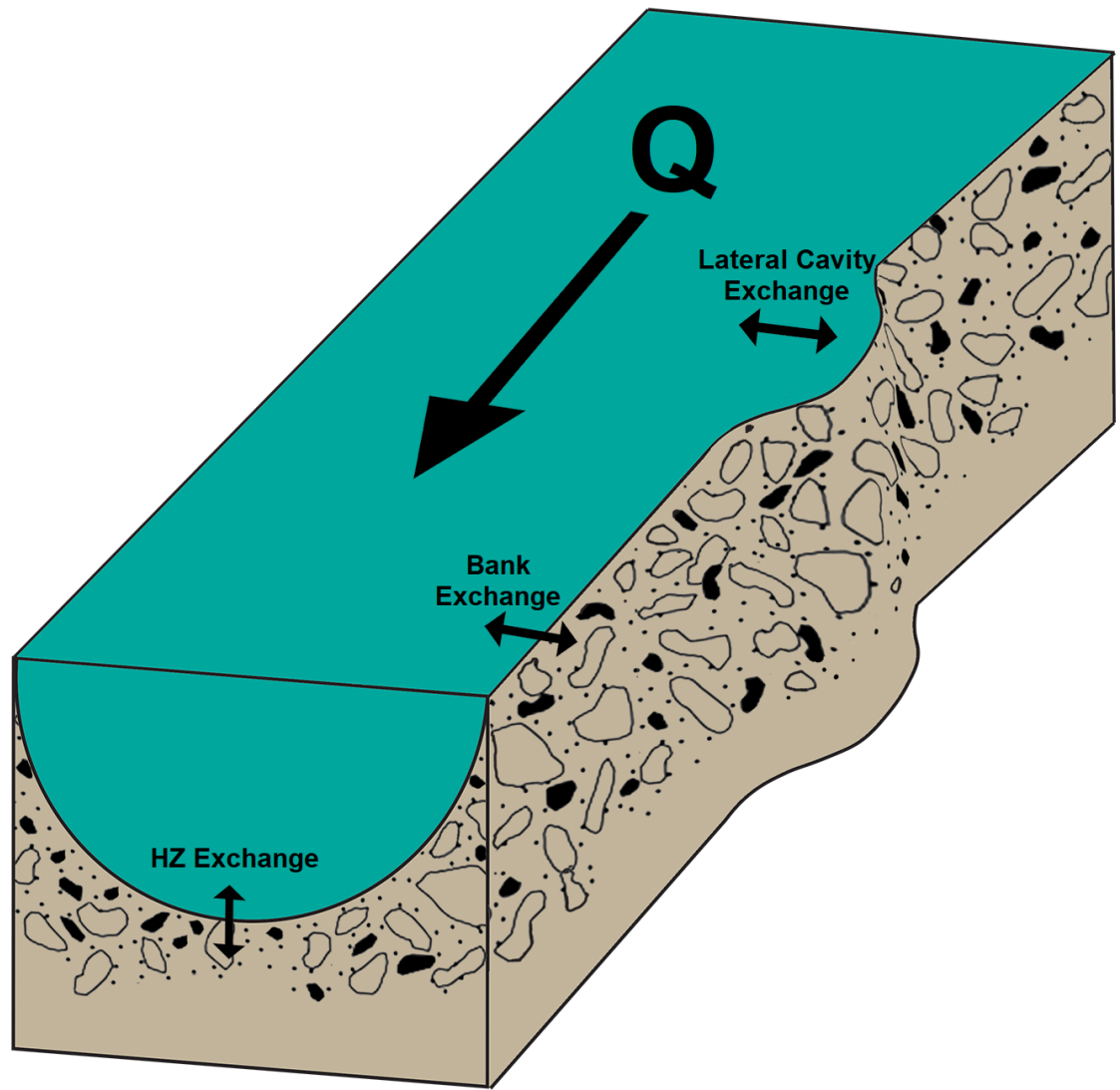


Figure 3.) Basic conceptualization of a mass balance with subsurface exchange. Q refers to the main channel flow. Lateral cavity, bank, and HZ exchanges are portions of the main channel flow that get removed from flow temporarily but are re-introduced to Q by the conservation of mass principle. Image based off of Harvey et al., 2000.

Objective

The objectives of the project were to characterize variability in transient storage zone processes and residence times in a small stream and relate the identified storage zone processes to observed physical characteristics of the stream.

A variety of field data collection and experimentation methods were used to characterize the hydrologic processes in Miller Run. The focus was specifically on the surface water, groundwater interactions, and transient storage zones in different sections of the creek. Data analysis and modeling were used to determine potential links between land use, stream management, and residence times in transient storage areas such as the hyporheic zone. The results contribute to further understanding of transient storage zone processes in relation to more easily observable variables in small stream systems.

Location and Site History

Miller Run (shown in Figure 4) was chosen as the study location due to close proximity to Bucknell University and the diverse physical characteristics along its route. It is located mainly in East Buffalo Township and partially in the borough of Lewisburg, PA . The stream is roughly 1.9 kilometers long with a 2.28 km² watershed (<https://streamstats.usgs.gov/ss/>). Miller Run joins Limestone Run in the Borough of Lewisburg which flows into the West Branch of the Susquehanna River.

Historically, Miller Run was adjacent to logging and agricultural usage and most of the surrounding forested area was cut down by 1820. Currently, most of the watershed that drains to Miller Run (see Figures 4 & 5) is owned by Bucknell University, and the university has manipulated the natural stream channel extensively. A golf course was built in 1930 and currently covers roughly 0.57 km²

and several sections of Miller Run were diverted using pipes. In some sections, the stream was confined to one channel to decrease channel migration and to keep golf and surrounding athletic fields maintained (Schaffer, 2008). Miller Run receives a large portion of the stormwater runoff from the Bucknell campus. Therefore, this small and highly channelized stream receives runoff and storm water drainage quickly running off the impervious surfaces of campus. The result is a stream that experiences sharp peaks after precipitation events and increased suspended sediment delivery, resulting in regular flooding along the river stretch (Schaffer, 2008). Excess runoff is common after the placement of impermeable areas of roadways and parking lots to accommodate visitors, piping of channel flow on the golf course and baseball fields, and the absence of riparian vegetation (Schaffer, 2008).

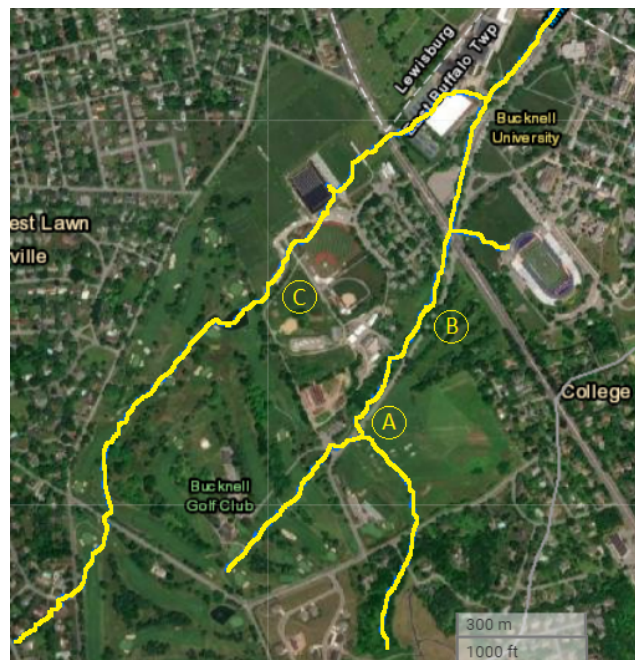


Figure 4.) Overview of Miller Run showing the channel running past the Bucknell Golf Club via StreamStats (<https://streamstats.usgs.gov/ss/>).

Miller Run has been the site of several student and class research and design projects. Breden (2012) summarized studies from 2008 to 2011, including classwork, and student researcher involvement from various departments. Alison Schaffer was the first major project attempting to understand the health of Miller Run, and several follow up course projects in 2009 and 2010, a course (UNIV 298 - Stream Restoration) lead by Craig Kochel (professor, geology) and Matthew McTammany (professor, biology) continued research to understand Miller Run. A data evaluation by Oudam Meas and Richard Crago (professor, civil and environmental engineering) in 2010 developed a conceptual plan for restoring Miller Run and further looked at available streamflow data and collected data used in the studies of Schaffer (2008) and Burke et al. (2009) to create a water budget. Carolyn Breden's own project was focused on establishing regular monitoring of the stream during the year and the creation of an accurate hydrologic and water quality model.

In 2013, Jonathan Algeo with the help of Rob Jacob (professor, geology) conducted a project utilizing GPR to monitor soil water content in clayey soils before and after storm events within the Miller Run floodplain. Multiple geophysical methods were used to find depth to bedrock, but only GPR data was used in examining the vadose zone. The site with the highest clay-rich layer present was used in their study, and GPR data, based on decreasing velocity with higher water contents, were used to estimate the presence of water. They suggested that this might be of application in future stream restoration efforts.

More recently, restoration efforts have been implemented in several sections of Miller Run. For example, there was a section of the creek that was piped under the driving range for a distance of approximately 80 m. This pipe was removed and the creek was daylighted and rerouted. Part of this project also included improvements to the surrounding watershed land use and restoration of the riparian buffer in several sections of Miller Run in this vicinity. In general, improved maintenance practices in some sections of the creek have led to healthier riparian areas in addition to recent tree-planting efforts.

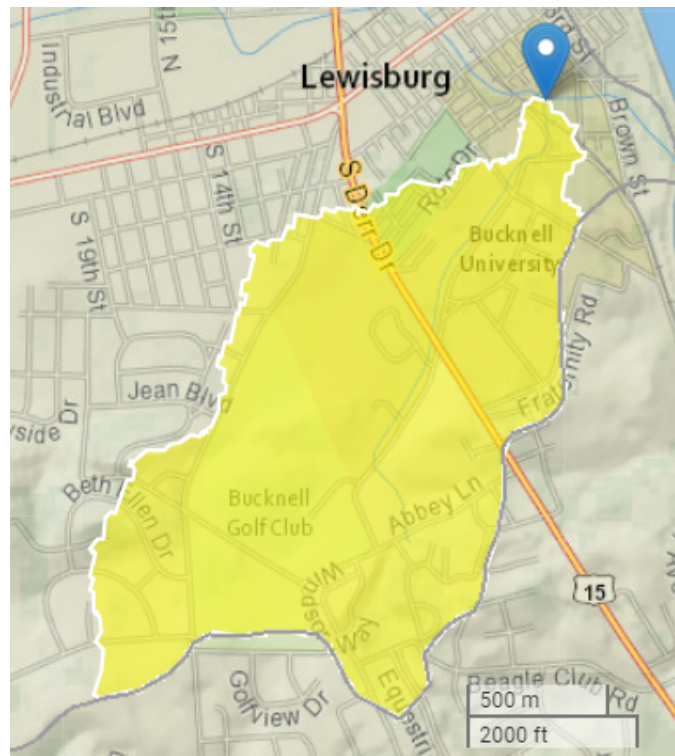


Figure 5.) Overall watershed that Miller Run drains (<https://streamstats.usgs.gov/ss/>).

Three potential study sites were chosen based on existing riparian zones and expected differences in physical characteristics of channel and TSZs . Figure 6

has satellite imagery of each site where A has riparian zones on both banks, B is immediately downstream with a riparian zone only present on the right bank, and C showing a tributary that lacks any riparian vegetation and is clearly a straightened channel section. The locations of sites A (near Sunflower Daycare and upstream of Art Barn Drive), B (downstream of Art Barn Drive), and C (a tributary to Miller Run at West Fields) are also indicated on the larger map of Miller Run in Figure 4.



Figure 6.) Aerial Imagery taken from Google Earth showing different parts of Miller Run. A) Proposed study site near Sunflower Child Care Center, upstream of Art Barn Drive. B) Downstream of Art Barn Drive. C) A tributary of Miller Run at West Fields.

Methods

A combination of data collection, field experimentation, and model simulation was used to meet the objectives of this project. Data collection included characterization of the study sites' physical characteristics. Field experimentation involved collection of geophysical data, repeated conservative tracer studies with continuous injections and related data collection. Based on the field

experimentation results, model simulations were created to characterize the hydrologic processes occurring in the transient storage zones (TSZs).

Site Investigation

Prior to performing tracer studies at the selected site, the physical characteristics were identified and measured. The physical characteristics of interest include many of the features shown in Figure 1 (e.g., presence of vegetation, lateral cavities, bed sediment, and obstacles). The extent of riparian vegetation was recorded. The watershed area and land use characteristics were determined using the USGS StreamStats tool and verified through field observations. Soil information came from the NRCS WebSoilSurvey tool and was used to interpret geophysical data once collected.

The collection of detailed site characteristics aided in the planning of tracer studies by identifying key transient storage characteristics of the study sites. These data also provided explanatory variables for any differences observed in the transient storage processes as a result of conservative tracer studies and model simulations.

Geophysical Methods

The field experimentation plan included attempting to collect electrical resistivity (ER) data concurrently to the tracer studies on Miller Run. Electrical resistivity has been used in groundwater studies by several researchers. Seismic refraction, magnetics, radioactivity, gravity, and electromagnetic methods have all been used to study groundwater (Adagunodo et al., 2018). These methods can be used to

outline aquifers, to determine overburden thickness, and to identify the underlying geologic topography of an area (Adagunodo et al., 2013).

Based on literature and available methods, the use of electric resistivity (ER) and ground penetrating radar (GPR) is anticipated to supplement the tracer field experimentation studies. Pairing of geophysical data with tracer data can be complementary to modeling flow and behavior. Ward et al. (2010b) used a pairing of ER, spaced over 20 meters, and an electrically conductive stream tracer to image the HZ during tracer studies. Although the chosen tracer for this study is not NaCl, it may be a valid set up and showed that ER data could actively image stream tracers within small streams (Ward et al., 2010b).

ER can track tracer concentrations through a streambed with a good enough temporal resolution that the limiting window of detection associated with tracer loss in long flow paths can be overcome (Ward et al., 2010a). The sensitivity of resistivity could be advantageous to create a more detailed delineation of the HZ and temporally related data. Comparison between field collected tracer samples and ER modeling revealed that ER underestimated the amount of solute present in samples, but temporal data agreed closely. The potential of correlating ER and solute data to produce a more accurate TSM was high.

Based on the possible usage of GPR and ER, site C was chosen to test GPR due to a low amount of vegetation while ER was planned sites B and C. The two preliminary ER setups at sites B and C were completed to test the feasibility of collecting geophysical data during a tracer injection. Two multi-electrode lines

were available each with 28 electrodes. With 56 electrodes, a grid of 4x14 electrodes was decided upon. Electrodes were placed at 1 meter increments between each other. Final grid dimensions were 3 meters wide and 13 meters long as shown in Figure 7. The planned grids were centered on the stream and the length extended downstream as it would cover a reasonable segment of the stream and would capture flow during tracer injection.

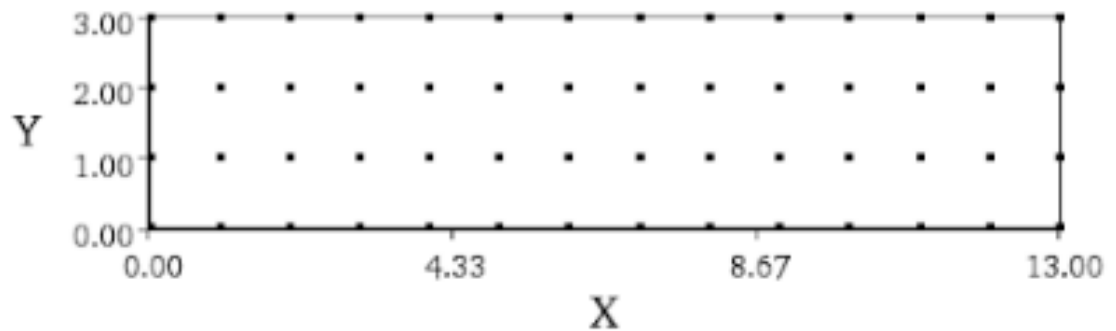


Figure 7.) Electrode grid used at both sites B and C where each dot is an electrode spike and the axes values are lengths in meters.

Contact probes were placed in the field after careful measurements to ensure correct spacing and inserted roughly halfway to inject current into the earth (Figure 8). Gravel and tree roots mildly interfered with exact placement however all spikes were placed within ± 10 cm of the exact location. Tree roots and gravel have a higher resistivity than the surrounding soil which resulted in slightly higher apparent resistivity values registered near these objects. The resistance values were within acceptable range and below 1,000 Ohm-m, so there was no anticipated interference during measurements.



Figure 8.) Basic setup that shows correct spacing. Yellow cables are the electrode lines that are resting on contact probes.

Ground penetrating radar (GPR) uses high-frequency electromagnetic (EM) waves directed into material and reflected signals to capture subsurface materials, voids, and differing material compositions (Huisman et al., 2003). Although most commonly used to find buried objects, it has also been successful at mapping water tables, unconfined aquifers, and underground rivers. GPR may not be directly applicable to HZ behavior, but it has been used to estimate water table depths and groundwater flow patterns by Manu et al. (2014).

Frequencies from 2.6 GHz to 10 MHz are often used for GPR depending on the desired resolution and depth. Lower frequencies penetrate deeper but have a lower resolution, but higher frequencies have shallower depths but have finer

resolutions. The decisions involved in selecting frequencies are dependent on how deep a target item may be and the significance for resolution. Survey setups include common-offset (COP) and common mid-point (CMP). During a common-offset survey, the transceiver and receiver are placed at regular intervals along the line, but are always a constant distance apart from each other. A common mid-point survey involves selecting a central location and then moving the transceiver and receiver outwards at regular measured intervals. COP was the chosen set up at Site C.

Four fixed-offset GPR lines using a trolley (Figure 9) were planned at Site C because of interest in collecting information on the water table under the stream. 500 mHz transducers provided the correct depth and resolution based on soil composition and depth to bedrock information from the WebSoilSurvey (<https://websoilsurvey.nrcs.usda.gov/app/>). A low frequency was ideal for data collection as lower frequencies have lower resolution but can penetrate deeper to reach bedrock. Water table levels would be identifiable by the high reflection value that water has compared to earth material.



Figure 9.) GPR setup using a trolley to hold the transceiver and receiver. Photo courtesy of Rob Jacob.

Tracer Studies and Modeling

Tracer studies are intensive field experiments that can yield substantial information about the residence times of different flow paths in a stream system. A constant-rate injection method (or continuous-injection), rather than the slug-injection method, was used for the conservative tracer studies. The tracer was injected at a small constant rate using a pump that ensured a uniform injection rate for the time period of injection. Downstream of the injection site, repeated samples were taken at identified distances from the injection and at consistent and recorded time intervals. Figure 10 shows an example injection setup and a downstream sampling location. The concentration of the conservative tracer solute in each sample plotted as a time series forms

breakthrough curves (or concentration-time curves). The shape of the breakthrough curves gives an indication of the hydrologic processes and interactions with TSZs in the study reach (see Figure 11). It is critical to obtain the optimum distance and elapsed sampling times so that an accurate plateau concentration can be reached as the plateau is important for determining several hydrologic processes (Kilpatrick and Cobb, 1984).



Figure 10.) Example tracer injection and sampling site. Injection happened at the white table and samples were collected downstream at the orange flag and at additional locations not shown in the image.

Bromide is a conservative tracer that is commonly used in soil-water projects and was used to determine the flow pattern of Miller Run. Prior tracer studies that

have been performed on Miller Run by Professor Newlin's classes have tried using both bromide and chloride as the tracer element. However, the background concentration of chloride in parts of Miller Run is higher and makes it more difficult to use. The bromide (KBr) tracer would be set up as a continuous injection, and downstream sampling locations were determined based on the results of the initial site characterization. Additionally, samples from different storage areas in the surficial TSZ observed along the study reaches as well as from the shallow bed sediments were collected to verify model simulation results. In order to have the best chance of being able to identify hydrologic processes of multiple TSZ in a reach, it was important to collect sufficient samples in the main flow and in the TSZs.

The results of field solute tracer studies are always specific to the hydrologic conditions at the time of the study. Therefore, tracer studies were repeated on the same sections of a stream under different hydrologic conditions and additional observations of physical characteristics were collected. Streamflow was measured with an electromagnetic flow meter and wading rod to estimate the concentration of tracer injectate that would be needed. Tracer study samples were placed in 20 mL plastic scintillation bottles for processing with the Ion Chromatograph in the Environmental Engineering and Science Lab (EESL) under the guidance of Monica Hoover (Director of EESL).

OTIS Modeling

Transient Storage Models (TSM) are commonly used to visualize the stream-catchment continuum as a finite reservoir composed of well-mixed solution that simplifies the stream flow and interaction with TSZs into a 1-dimensional model (Bencala et al., 2011). The TSM modeling approach is one of several that have been studied in past literature and summarized by Boano et al. (2014). These models simulate downstream flow with a 1-dimensional advection-dispersion equation that allows for lateral inflow and interaction/exchange with a surface or subsurface TSZ (Packman and Bencala, 2000). OTIS (One-dimensional Transport with Inflow and Storage) has been reliably utilized in modeling hydrologic processes and is ideal for studying transient storage processes for this project (Runkle, 1998). After the data from the tracer studies were collected, TSMs were constructed to fit the observed tracer breakthrough curve data by adjusting stream and TSZ parameters to understand stream characteristics. Figure 11 shows an example of the general shape of breakthrough curves from a tracer study. Runkle (2000) suggests that a TSM can estimate how much mixing is due to differing types of TSZs such as streambed morphology. Adaptations of the OTIS model have been developed to help identify processes due to the presence of multiple TSZs that may have different characteristics and rates of exchange.

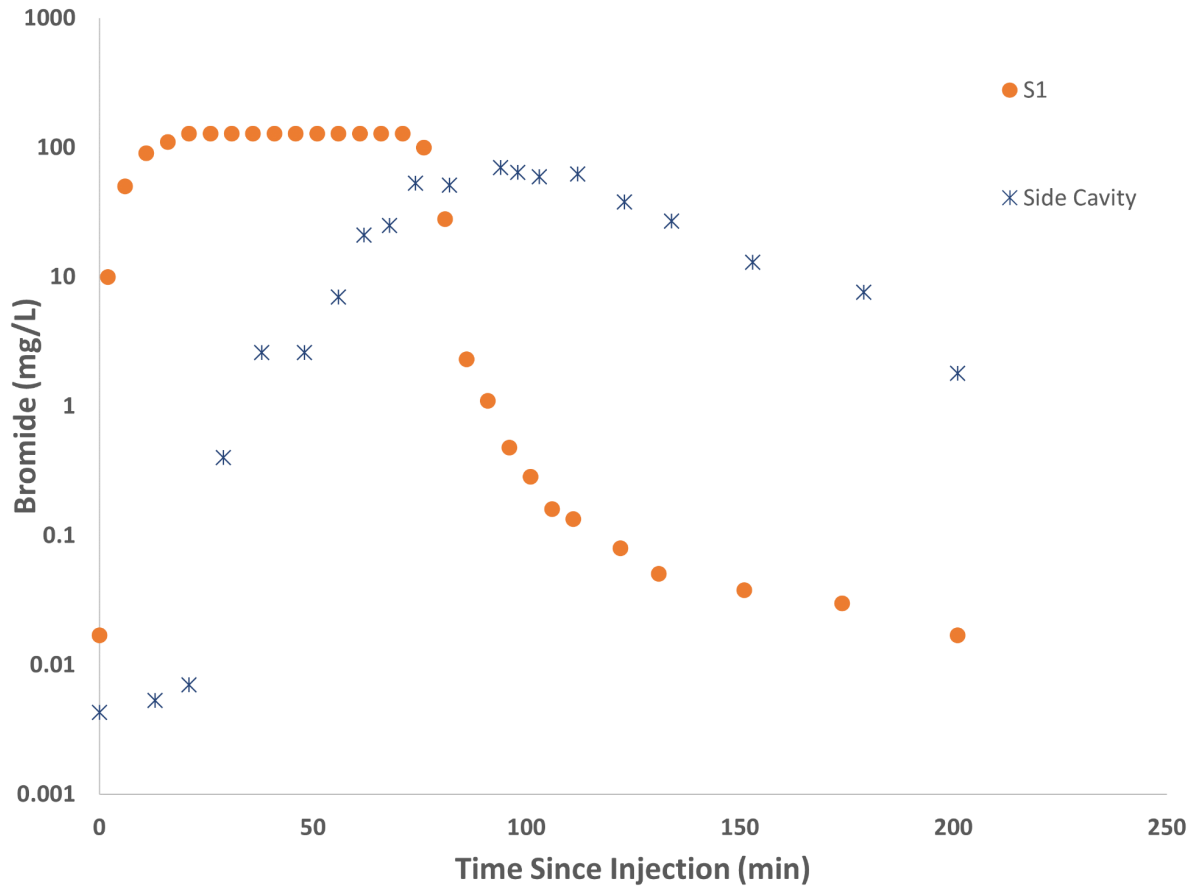


Figure 11.) Breakthrough curves at two different sites using bromide as a tracer. The measured tracer concentration is represented by the points on the plot.

The OTIS model uses the advection-dispersion equation in the main channel and includes an extra term to simulate exchange with a TSZ. The models are capable of simulating first-order decay and sorption, but a conservative tracer is used for this study so these terms are not included in the following discussion of the governing equations. An original functionality of a companion executable to OTIS, OTIS-P, is that OTIS-P is capable of parameter estimation to identify values of variables that can describe systems where tracer study breakthrough curves are measured (Runkel, 1998). Different hydrological variables that are

able to be estimated include dispersion (D), main channel area (A), storage zone area (A_s), and exchange coefficients (α). OTIS-P uses the non-linear least squares (NLS) regression to determine the best fit parameters (Runkel, 1998). The NLS regression uses the Standards Time Series and Regression Package (STARPAC), a library of Fortran subroutines designed for NLS regression of which 12 are designed for estimation (Donaldson and Tyron, 1990). OTIS-P couples the OTIS model and STARPAC and allows the user to control which variables should be held constant and which should be estimated.

An extension of OTIS and OTIS-P is OTIS-2Stor. With OTIS-2Stor, the mathematical model is extended to include two TSZs (Choi et al., 2000). OTIS-2Stor is an adapted module of OTIS that is intended to offer extended ability to identify two TSZs from observed data instead of a single zone. OTIS-2Stor has the added capability of estimating parameters for a second storage zone, the ability to fix parameters in one reach and estimate them in another, and the use of non-linear least squares parameter estimation with weights on the observed data (Newlin, personal communication, 2023; Choi et al., 2000).

OTIS-2Stor uses the same basic governing equations as the OTIS software created by Runkel (1998) but has been manipulated by the addition of a second storage zone. It also has the ability to calculate reactive transport, including first order decay and sorption in the main channel. Only solute exchange occurs between the main channel and each storage zone, and there is no exchange simulated between the TSZs.

Equation 1 is a tracer mass balance equation that uses advection, dispersion, lateral inflow, storage exchange between the storage zones and the main channel.

$$\frac{\partial C}{\partial t} = -\frac{Q}{A} \frac{\partial C}{\partial x} + \frac{1}{A} \frac{\partial}{\partial x} \left(AD \frac{\partial C}{\partial x} \right) + \frac{q_{Lin}}{A} (C_L - C) + \alpha_1 (C_{S1} - C) + \alpha_2 (C_{S2} - C) \quad (1)$$

The equation is written where:

C - main flow zone solute concentration [M/L³]

C_L - lateral inflow solute concentration [M/L³]

Q - volumetric flow rate [L³/T]

A - main flow cross-sectional area [L²]

D - dispersion coefficient [L²/T]

q_{Lin} - lateral inflow rate [L³/T-L]

C_{in} - lateral inflow solute concentration [M/L³]

α_1 - storage zone 1 exchange coefficient [/T]

C_{S1} - storage zone 1 solute concentration [M/L³]

α_2 - storage zone 2 exchange coefficient [/T]

C_{S2} - storage zone 2 solute concentration [M/L³]

t - time [T]

x - distance [T]

Equations 2 and 3 are tracer mass balance equations for storage zone 1 and storage zone 2.

$$\frac{dC_{S1}}{dt} = \alpha_1 \frac{A}{A_{S1}} (C - C_{S1}) \quad (2)$$

$$\frac{dC_{S2}}{dt} = \alpha_2 \frac{A}{A_{S2}} (C - C_{S2}) \quad (3)$$

where

C - main flow zone solute concentration [M/L³]

α_1 - storage zone 1 exchange coefficient [/T]

C_{S1} - storage zone 1 solute concentration [M/L³]

α_2 - storage zone 2 exchange coefficient [/T]

C_{S2} - storage zone 2 solute concentration [M/L³]

A_{S1} - storage zone 1 cross-sectional area [L²]

A_{S2} - storage zone 2 cross-sectional area [L²]

t - time [T]

As the equations that OTIS-2Stor uses are partial differential equations (PDE), the implicit Crank-Nicolson method is used to find numerical solutions (Runkel, 1998). Two boundary conditions must be defined to produce a solution. The

upstream boundary conditions are fixed concentrations of the injected solute that is entering the upstream stream segment (Runkel, 1998). The downstream boundary condition is a fixed dispersive flux between segments i and $i+1$ where a user-supplied value is input set at the $i+1$ segment after the last segment i (Runkel, 1998). For this study, the user supplied value for the dispersive flux was the background level of Bromide. However, the modeled reach was extended sufficiently downstream to minimize the impact of the downstream boundary condition on the modeled solution where breakthrough curves are available for comparison. OTIS-2Stor has the capability to solve with steady flow and unsteady flow conditions, but for the purpose of this work steady flow was used.

To determine the best-fit parameters for the TSZs, both a trial-and-error approach and use of the non-linear least squares (NLS) method were used with the OTIS-2Stor model and compared to the collected breakthrough curve data. The observed data were plotted against simulated breakthrough curves generated by OTIS-2Stor.

With the knowledge that certain parts of the breakthrough curve (Figure 11) correspond to particular parameters such as exchange rates, dispersion coefficients, and areas, the assumption is that variables can be manipulated independently until the estimated values are correct. The plateau of OTIS-2Stor generated curves corresponds primarily to the lateral inflow of groundwater (q_{Lin}) while the slopes of the plateau shoulders are controlled by the stream's

cross-sectional area (A) as explained by Jones and Mulholland (1999). The tail of the breakthrough curves represent the TSZ's exchange processes.

Results and Discussion

Site Investigation

Detailed site investigations took place during the Summer of 2022. A combination of physical measurements and observations were used in conjunction with data provided by government agencies such as the NRCS's WebSoilSurvey and riparian buffer maps for verification and quantification of observations.

Based on WebSoilSurvey data of the area (Figure 12), a typical soil profile was developed. The map unit that all of the study sites are in is called the Edom complex (EdB) that has 4 layers in the typical profile. Three soil horizons are found in the Edom complex H1 has a depth of 22.86 cm (9 in) and is a channery silt loam, H2 is 22.86 to 99.07 cm (9 to 39 in) deep of channery silty clay loam, and H3 is 99.06 to 152.4 cm (39 to 60 in) in depth of very channery silty clay loam. Channery soils have thin, flat fragments of the bedrock within them. Estimated depth to bedrock was approximately 1.5 m (60 in). The sites are in the Keyser and Tonoloway and Wills Creek formations. These formations are predominantly limestone. Keyser and Tonoloway formation is interbedded with shale, while the Wills Creek formation has a mix of shale, siltstone, and sandstone throughout.



Figure 12.) WebSoilSurvey showing soils present at all of the sites (<https://websoilsurvey.nrcs.usda.gov/app/>).

During the Summer 2022, different types of potential TSZs were identified at all of the sites. Due to low water levels, Site B had priority when cataloging TSZs and it was identified as the location of the first potential tracer site given that hydrologic conditions improved there first. Several TSZs were found and noted at Site B, including instream vegetation, submerged objects, and a lateral cavity. These TSZs were marked with flags to be considered for TSZ sampling locations during a future tracer study. More details about the TSZs at each site are given in the following text that provides more details about each site individually.

To supplement field investigations, riparian buffer zone data from the Chesapeake Conservancy’s Conservation Innovation Center (Chesapeake Conservancy, 2019) was used. Detailed land cover raster data is available for 30.48 m (100-ft) riparian buffers along streams in the Chesapeake Bay watershed which includes Miller Run and its tributaries. The land cover in the riparian areas of each of the sites are shown in Figure 13. This information was quantified by area and presented for each study site in the following text.

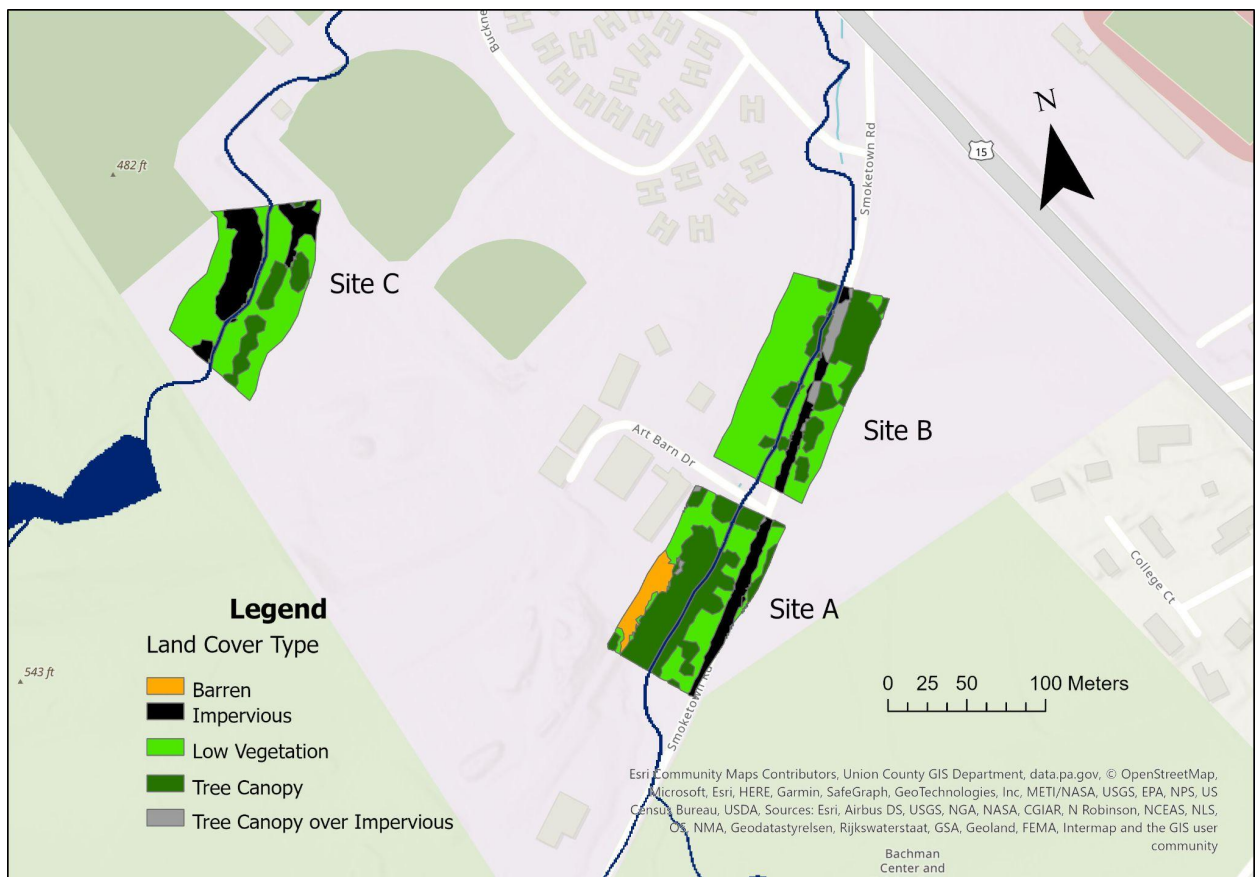


Figure 13.) Riparian buffer map of Site A, Site B, and Site C showing 30.48 m (100 ft) wide buffer.

Site A

Site A had multiple distinct and unique features and TSZs within the stream itself not found at the other sites as it was the most restored segment of Miller Run. It was heavily vegetated with large trees and bushes compared to Sites B and C. On the most upstream section of Site A that was proposed for the tracer study, the main segment of Miller Run meets with a side channel seen in Figure 14 below.



Figure 14.) Main channel, left, of Miller Run meeting with a smaller side channel, right, that is ephemeral with small amounts of instream vegetation.

The larger stream was 1.25 m (4.1 ft) across and the smaller branch was 0.37 m (1.2 ft) wide. Velocity measurements were collected throughout the main Miller Run stream, with an average velocity of 0.097 m/s (0.318 ft/s) at the time of observation in early summer 2022.

The branches join together and flow over a narrowed segment with a riffle that feeds into a pool, 1.62 m (5.3 ft) wide, where the water's velocity dropped (Figure 15). The pool had several larger submerged obstacles of large cobbles and instream vegetation.



Figure 15.) Pool segment of Miller Run in Site A. The riffles can be seen in the upper right corner of the background.

Following these sections of Site A, the stream flows through a heavily restored area. Several objects were present within Miller Run that act as TSZs including logs and cobbles. A clear image of the stream conditions in the restored section is found in Figure 16. There were multiple cobbles underlying the logs and extending into the pools, as well as bricks and cement blocks as obstructions in the main flow channel.



Figure 16.) Restored pool (left) with logs emplaced to create a series of pools with submerged objects. Bolted in bank protection is visible in the upper left background. The water from the pools flows under the logs placed in the stream to the downstream pool (right). A portion of the flow is also diverted by a pipe. The two pools are separated by a large assortment of cobbles which then flow towards Site B through a riffle.

The most downstream section of Site A separated into two pools. The left pool which is directly under the log and pool complex was 1.37 m (4.5 ft) wide, 20.37 cm (8.02 in) deep, and was stagnant. The right pool was 1.19 m (3.9 ft) in width

and 8.20 cm (3.23 in) deep. It had a velocity of 0.007 m/s (0.022 ft/s). Depths throughout the entire stream varied from 1.524 cm (0.6 in) to 4.7 cm (1.85 in).

Information based on the riparian buffer of 30.48 m (100 ft) extending on either side of Miller Run was used to create estimates of the percent of land use in five categories. These included barren, low vegetation, impervious surfaces, tree canopy, and tree canopy over impervious surfaces. The results (Figure 17) show that Site A is predominantly tree canopy and low vegetation in the 30.48 m (100 ft) riparian buffer zone with almost 50% tree canopy.

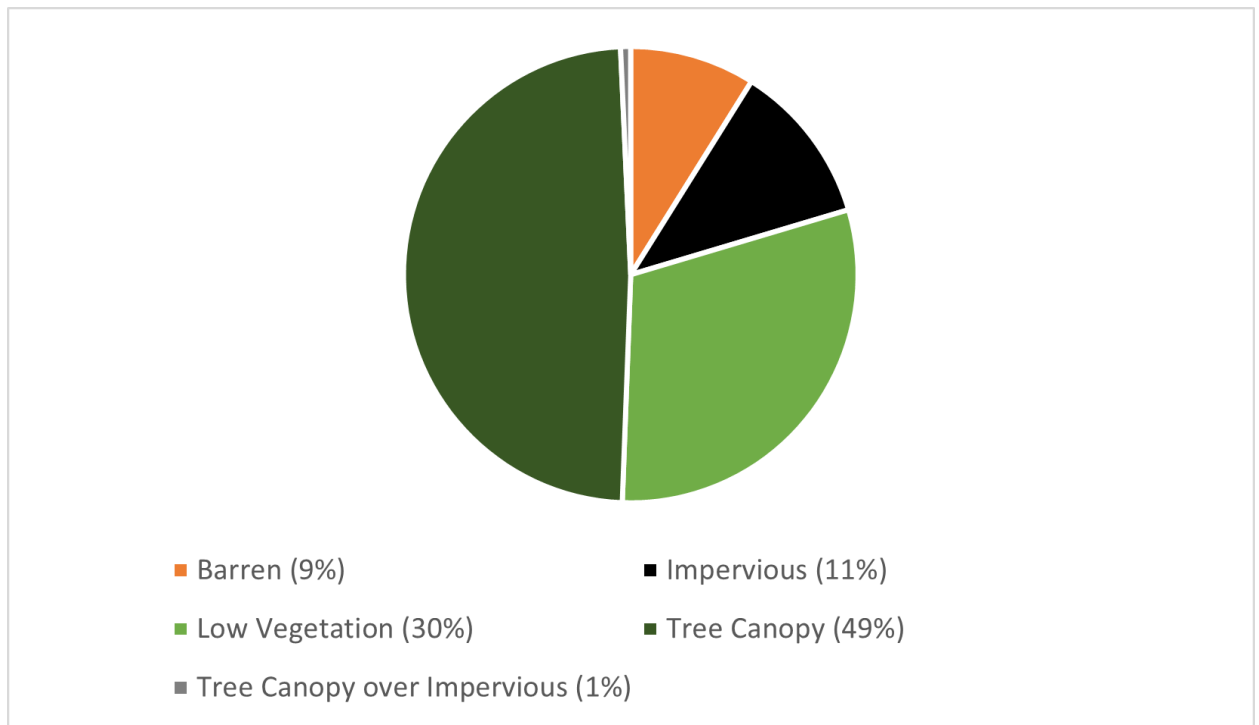


Figure 17.) Land cover present at Site A.

Site B

Downstream of Site A, Miller Run flows under a small bridge for Art Barn Drive, where it enters the designated Site B. Although Site B is directly downstream, the stream has very different physical and hydrologic characteristics.

During initial site investigations in the early summer 2022, the left bank and riparian area was in the midst of restoration involving the use of live stakes, planted trees, and no-mow areas that continued throughout the stream's length. These measures resulted in a higher amount of riparian vegetation than previously anticipated based on prior years. A mix of established trees, bushes, and grasses made up the bulk of the right bank and riparian area as restoration had begun earlier.

The stream entered a series of pools and riffles (Figure 18) interrupted by sections of small meanders. One of the pools that was measured was 1.725 m (5.66 ft) across and a nearby pool was of a similar width of 1.615 m (5.3 ft). Riffled sections had a larger range in widths, the smallest was 0.70 m (2.29 ft) and another was 0.72 m (2.36 ft).



Figure 18.) Upstream view of the upstream section of Site B. Riffles are visible in the section near the orange flag.

Depth and velocity measurements were also taken at various locations in early summer 2022. Riffles had depths of 29.9 and 29.4 mm (1.18 and 1.16 in). Average velocities across the riffles were 0.131 and 0.085 m/s (0.43 ft/s and 0.279 ft/s)

respectively. These measurements were taken near the first orange flag in Figure 18 and in the downstream end of Figure 19.

Visible in Figure 19 are multiple TSZs visible due to the low flow level. There are multiple submerged obstacles and instream vegetation. Not present during the tracer studies was algae that was visible in the Spring 2023, which can also act as a TSZ (Harvey et al. 2006).



Figure 19.) Obstacles within Miller Run at Site B (top). Submerged rocks and in-stream vegetation nearby (bottom). Algae growth was not present during the tracer studies.

A photo facing upstream from the last sampling location (Figure 20) shows the small meanders that Miller Run has. The same rocks, algae, and vegetation can be seen within. This downstream section of Site B had much steeper banks on either side from where the channel starts to become incised. According to the riparian buffer information (Figure 21) the bulk of land cover was low vegetation and tree canopy where almost 70% is identified as low vegetation. Impervious surfaces were due to Art Barn Drive and Smoketown Road.



Figure 20.) Looking upstream at the downstream section of Site B. Spring 2023 low flow shows a pool in the background that enters a narrowed section with multiple rocks and vegetation within.

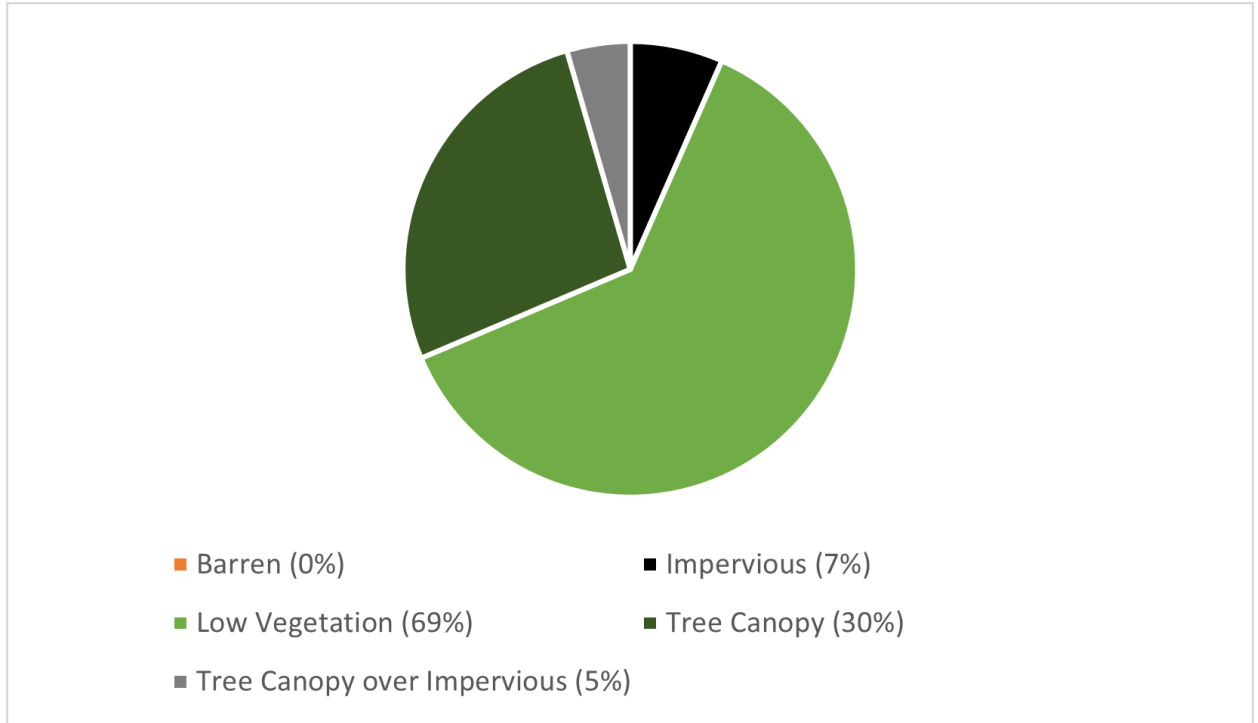


Figure 21.) Percentages of land uses in the buffer zone at Site B.

Site C

During the early summer 2022 site investigation of site C, most of this tributary of Miller Run was dry. Vegetation grew freely within (Figure 22) the small stream section that was measured to be 44.9 m (147 ft) in length. The width of the tributary was 57.2 cm (22.5 in) and remained fairly constant throughout.



Figure 22.) Tributary of Miller Run at Site C (left) showing the dry bed present during the site investigation. Vegetation growing on the stream bed (right) that grew heavily during the summer 2022.

The upper half of Site C had a small amount of water present (Figure 23) with a measured depth range of 2.28 cm (0.9 in) to 5.08 cm (2 in). It was found that the water was standing water with no velocity. There was a distinct separation between the dry and wet sections of Site C where the stream abruptly vanished. In the left photo of Figure 23, the division can be seen prior to the revealed rocks in the stream. This section was flagged for geophysical investigation to potentially see if subsurface characteristics were responsible for the dry stream.



Figure 23.) Left image is pointing downstream showing the abrupt cessation of flow. Right image shows shallow water found in the upstream portion of Site C.

There was a predictable lack of variety in the buffer zone at the tributary (Figure 24). There was a large parking lot nearby, while most of the surrounding vegetation was cut short. Eight large trees are spaced out along the right bank when facing downstream. Therefore, the land cover summary for the buffer is mainly low vegetation, with a more significant impervious surface cover (26%) than the other two study sites.

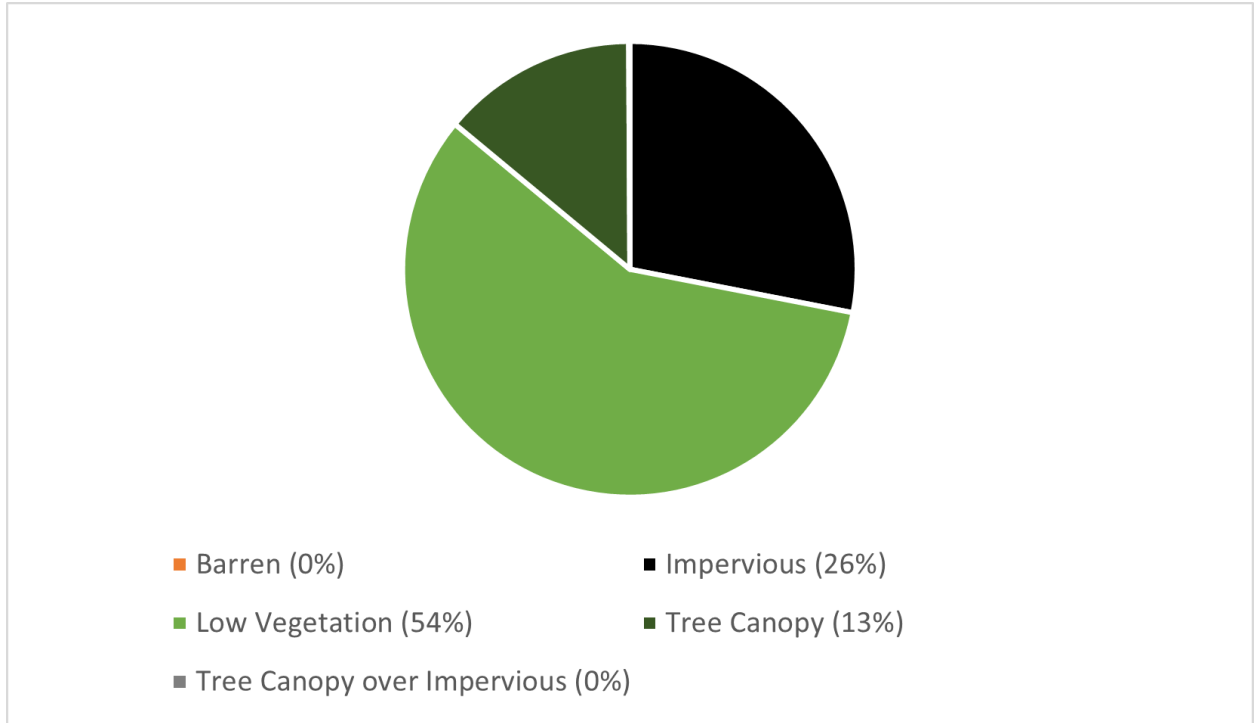


Figure 24.) Land cover found in Site C's riparian buffer zone.

Geophysics

Two of the sites had geophysical surveys done at them to test the capability of different equipment at these sites. Site C was the only site where the GPR method was able to be tested. Both sites B and C had trial runs of ER experiments done at them.

It is known that the ability for GPR to penetrate into material decreases as the water content increases. During data collection, the stream at Site C was full and surrounding soils were most likely saturated. The bedrock is relatively shallow at the location, so it was anticipated that a possible distinct difference between the stream, soil, and bedrock would be visible.

The results from multiple GPR lines were compiled into software to develop radargrams using traces. Traces or scans are vertical columns of data collected along a transect. The depth shown in traces corresponds to the depth that the pulses were able to reach. The radargrams were filtered and examined for hyperbolas or changes in velocities that would differentiate between the stream, soil, and bedrock layers.

Although the GPR traces did not provide any information on a water table interface, there was a small amount of information that could be taken from them. Some potential bedrock structure could be seen by the jagged black and white lines in Figure 25. The red markers in the lower right indicate that there was an error that the transceiver and receiver were not able to communicate. Faint hyperbolas, also in the lower right, have the same velocity as air.

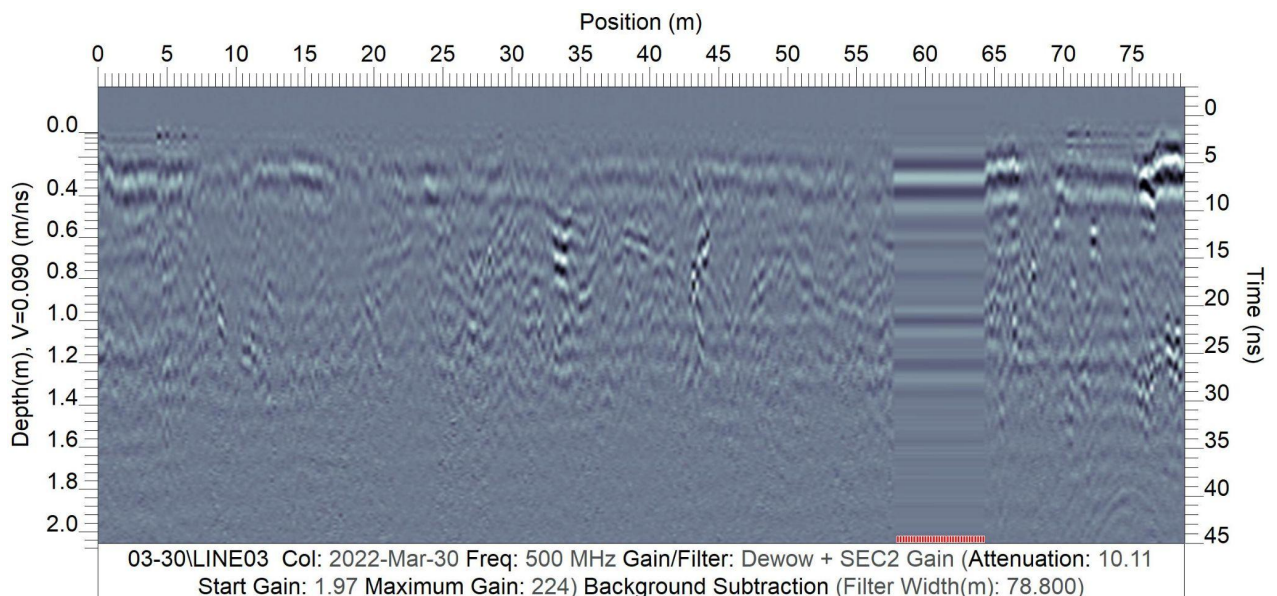


Figure 25.) Longitudinal GPR section at Site C. Jagged signatures possibly due to rough bedrock surface. Lower right shows hyperbolas that have the same velocity as air.

A different GPR line (Figure 26) that crosses the tributary did not have any distinct interfaces visible in the radargram. The left side displays a faint hyperbola that has a high velocity. This was interpreted to be caused by the presence of a large tree.

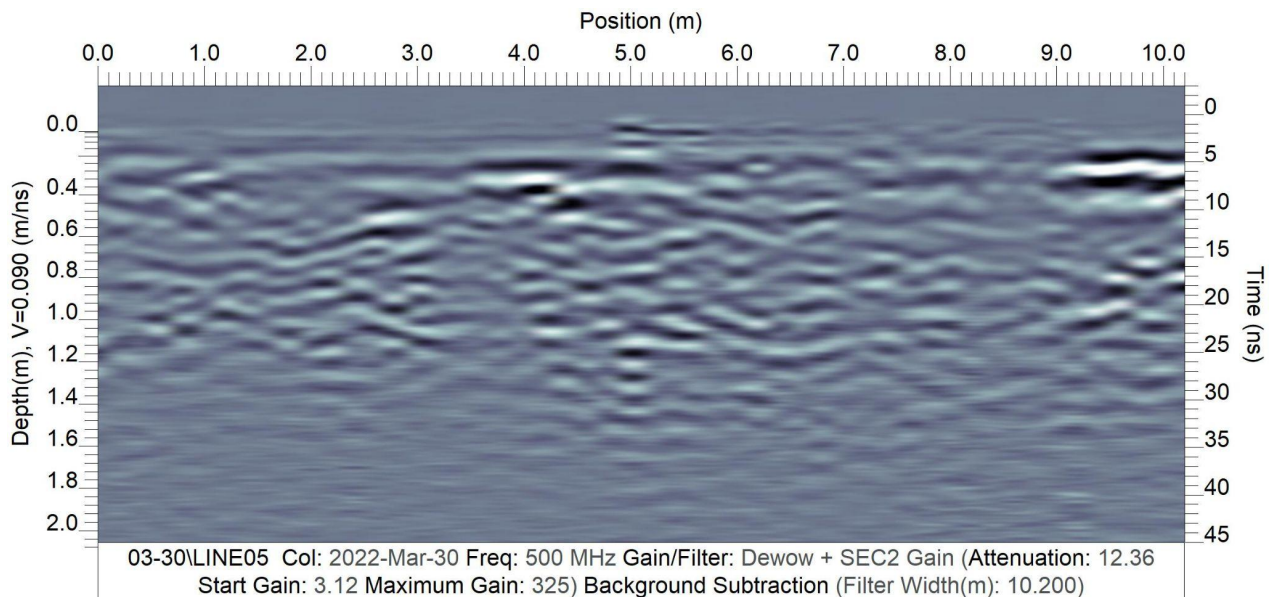


Figure 26.) A higher amplitude in the center of the tracer of a transverse line over Miller Run's tributary. Left side shows a large hyperbola near the surface that may have been one of the trees that line the right bank.

The radargram found below (Figure 27) has a clear increase in amplitude at the center, where the stream would have been crossed. There is a potential interface below at a depth of 1.2 meters.

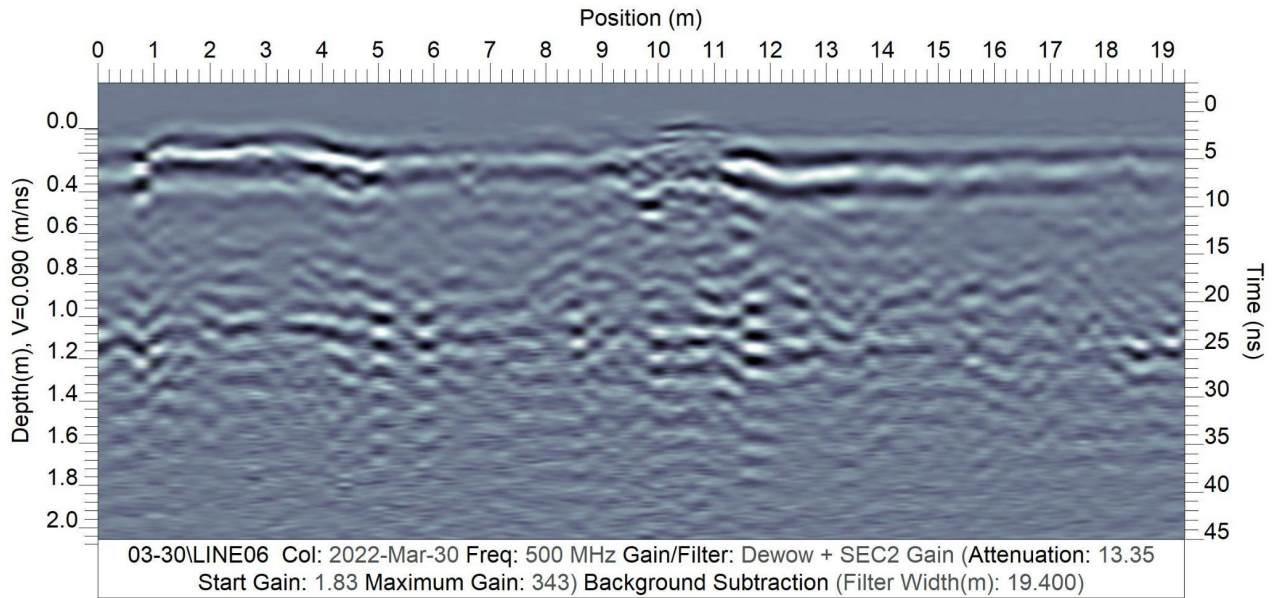


Figure 27.) Possible secondary interface.

Multiple radargrams (Figures 25-28) showed no differentiation between velocities or hyperbolas indicative of a submerged object. Most traces reached a depth of roughly 2 meters.

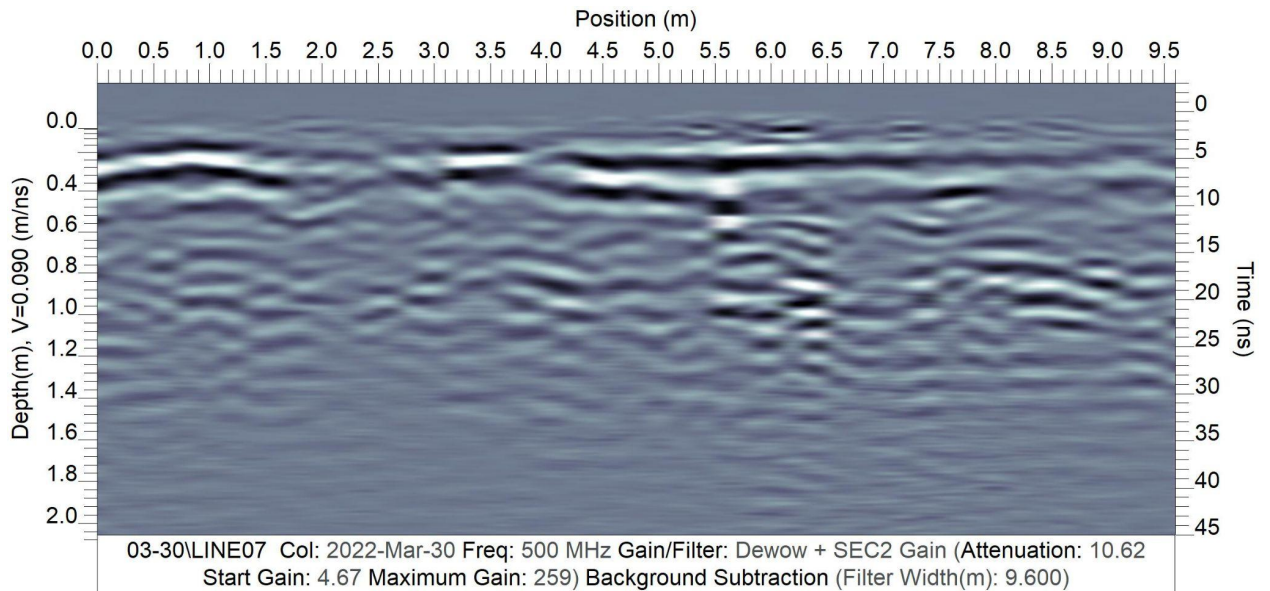


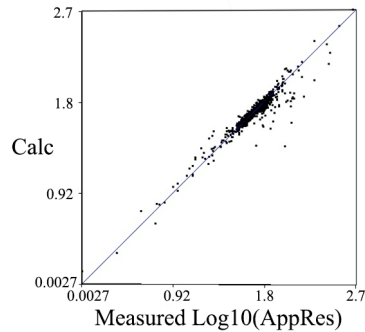
Figure 28.) Radargram from Site C showing limited data that lacks velocity differences.

After the GPR trial was determined to not provide additional data relating to the water table, it was decided to continue with ER data collection. The same setup was used at sites B and C at different times. The stream conditions were similar at both sites and the vegetation levels at both sites were also assumed to be similar to the conditions that would be present during the planned tracer studies.

When resistivity measurements were taken, current was able to penetrate 2.67 meters. When processing the raw data, a root mean square error (RMS) was used to determine if the resistivity data was within an acceptable range. The RMS is the difference between the measured and calculated resistivity values (Salam, et al, 2017). An RMS of below 10% was desired and the lowest RMS achieved was 5% after multiple iterations in the AGI EarthImager software. This was an acceptable RMS value. Resistivity crossplots showing the RMS values and amount of iterations are shown in Figure 29.

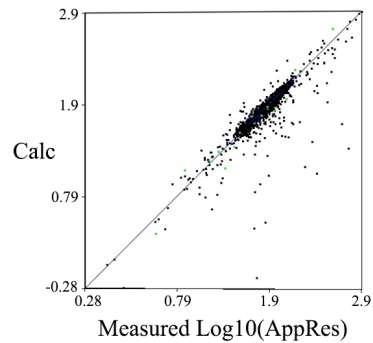
Visuals of the data (Figures 30 & 31) were created with the inverted resistivity (IR) images that were generated by the software. The depth of 2.67 meters extends further than the estimated bedrock height, so there was an expectation that bedrock characteristics would be visible on the IR images. Resistivity values on the images ranged from 2 Ohm-m to 100,000 Ohm-m. Such a large range would be expected with the presence of multiple materials.

Apparent Resistivity Crossplot



Iteration No. 18. RMS = 5.0%. L2 = 1.0

Apparent Resistivity Crossplot



Iteration No. 40. RMS = 10.7%. L2 = 4.6

Figure 29.) Apparent resistivity crossplots that have the iteration number and the RMS percent of the Site C (left) and Site B (right) ER data.

Based on the lack of subsurface penetration and features, the water table was most likely high and close to the surface which resulted in a severe reduction of subsurface information. Additionally, the heavily saturated soil most likely contributed to the lack of penetration from the GPR instruments.

Interpretation of IR imagery relied on the soil map information and resistivity ranges available in Table 2. It was assumed that the yellows and reds of higher resistivity values correspond to the bedrock. The estimated depth matches well with the known typical profile, and the hummocky surface was interpreted as the weathered surface of karst features.

Table 2.) Common geologic material present and the corresponding resistivity ranges.

Geologic Material	Common Resistivities (Ohm-meters)	References
Wet or moist clayey soil and wet clay	1 - 10	Burger (1992)
Wet or moist silty soil and silty clay	Low 10s	Burger (1992)
Wet or moist silty and sandy soils	10 - 100	Burger (1992)
Topsoil	50 - 100	Milsom (2003)
Clay	1 - 100	Milsom (2003)
Gravel	100 - 600	Milsom (2003)
Weathered bedrock	100 - 1000	Milsom (2003)
Sandstone	200 - 8000	Milsom (2003)
Limestone	50 - 10,000	Milsom (2003)

Based on the lack of subsurface penetration and features, the water table was most likely high and close to the surface which resulted in a severe reduction of subsurface information. Additionally, the heavily saturated soil most likely contributed to the lack of penetration from the GPR instruments.

Interpretation of IR imagery relied on the soil map information and resistivity ranges available in Table 2. It was assumed that the yellows and reds of higher resistivity values correspond to the bedrock. The estimated depth matches well with the known typical profile, and the hummocky surface was interpreted as the weathered surface of karst features.

Channery soil contains thin fragments or chips of the bedrock within the horizon. As the soil in the EdB unit is very channery, the fragments of limestone most likely increased the resistivity. The soil was most likely the green to yellow range of resistivity colors. There was no visible difference found on the surface of the inverted images that would have coincided with the stream.

At Site C(Figure 30), the bedrock was relatively shallow on the upstream end. The most downstream portion was primarily soil. This was also the section of stream where water simply vanished and it became a dry stream bed. It was assumed that the water was disappearing into the subsurface due to subsurface karst features and the bedrock tapering away would support this.

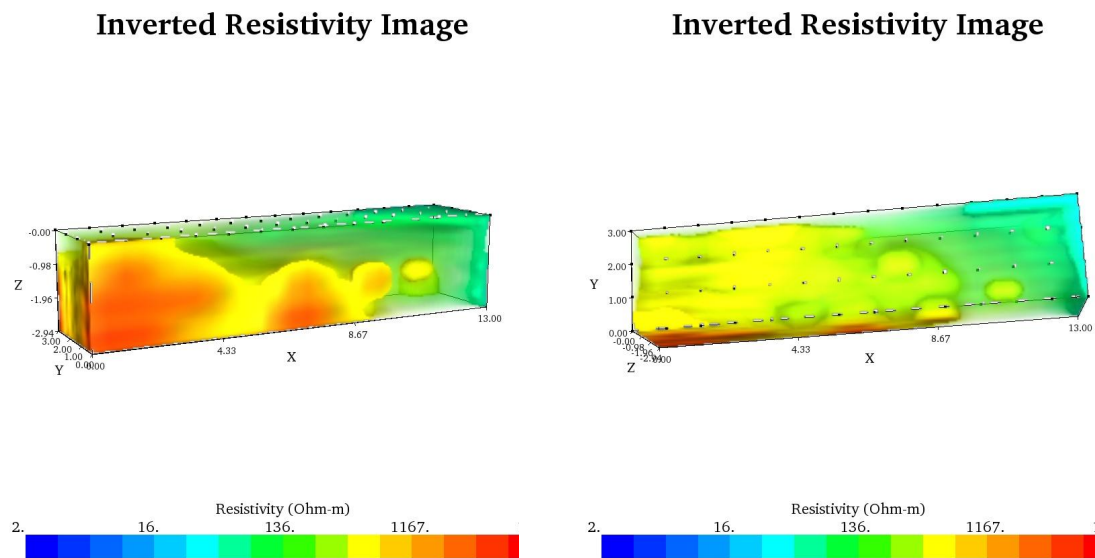


Figure 30.) Site C side view (left) and top view (right) semi-transparent images that show the higher resistivity values that correspond with bedrock in different perspectives.

For the imagery collected at Site B (Figure 31), the bedrock was also relatively shallow, but there was also more soil present. Soil was in the green range of resistivity values. RMS percentages were higher for Site B through all of the iterations run by the AGI EarthImager software. It was a higher percentage than Site C, but this was possibly due to a high, steep bank on the right that caused a vertical shift of the current. There was also more vegetation and roots present in the soil which can influence the resistivity (Giambastiani et al, 2021).

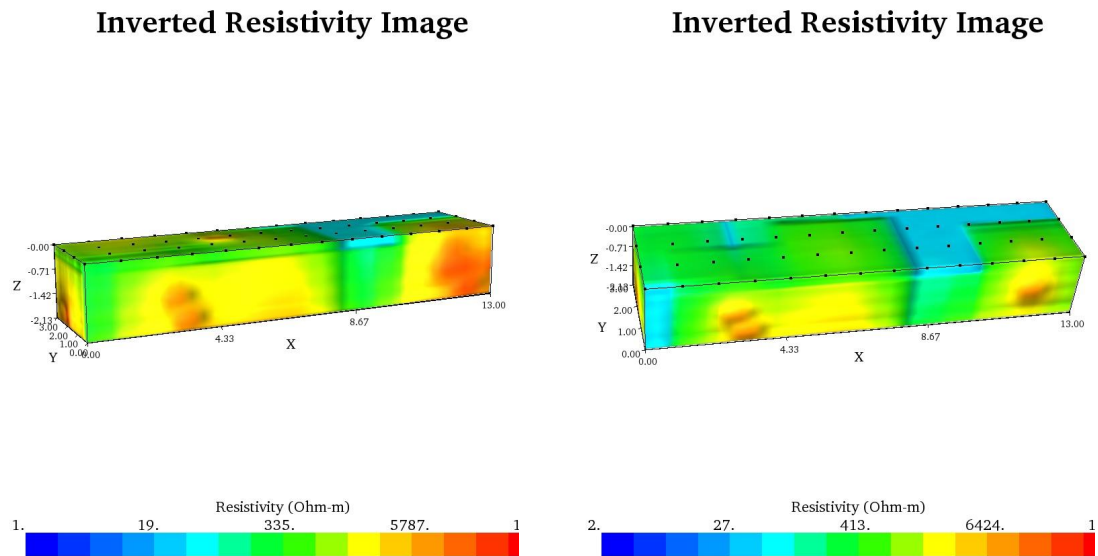


Figure 31.) Side view (left) and top view (right) of inverted imagery collected at Site B.

The lower range of values, blue colored in the images, most likely corresponds to wet clay and silt rich soils. The stream was mostly centered in the grid, but is not visible at all in the images similar to the previous Site C investigation. The likely cause of this was that the high resistivity materials were saturated with water that

has a high conductivity, so that distinct separation between background conditions and tracer breakthrough concentrations was likely not possible.

While the GPR failed at providing bedrock information, the ER data gave a more detailed understanding of the subsurface under the sites. The ER inverted resistivity images agreed with the available information from the WebSoilSurvey. While ER was intended to be used in conjunction with the tracer studies to give 3-dimensional subsurface data of the treated water traveling through the system, it was determined that it would not provide the desired information. This was most likely due to the highly conductive material found in the site and the high background concentrations of salt in the stream water. Making additions to the water to boost the conductance is common for tracer studies, but the existing salt content made it difficult to dose without causing disruption to the ecosystem and fauna living in the stream.

Tracer Studies

During the 2022 Summer, there was unexpectedly low rainfall. This resulted in drought conditions and the study sites were reduced to dry beds for most of the summer. Water levels improved at the end of August which allowed for two tracer studies when water was present at site B (at the end of September 2022 and in the middle of October 2022). Due to the lack of water, sites A and C did not yield enough connected water for any tracer studies. Some locations in Miller Run that had pools of water in the summer were tested with a rhodamine dye tracer to

determine if the pools were hydrologically connected. It was found that this was not a strong enough connection to attempt a tracer study.

Bromide was used as the conservative tracer for both tracer studies at site B. The first tracer study (September 2022) will be referred to as the B1 tracer study and the second tracer study (October 2022) will be referred to as the B2 tracer study. Multiple sampling locations were marked along the stream using survey flags to create some consistency between the two studies.

For the first tracer study (B1), the sampling locations were located along a small stretch of Miller Run that was 3.90 m (12.8 ft) long. Flow conditions were very low but a short connected reach was identified for a tracer study. The injection location and sites are visible in Figure 32. Sampling sites 1, 2, and 3 were identified as locations for surface water samples in the main channel section. Site 1 was 0.91 m (3 ft) away from the injection, site 2 was 1.74 m (5.7 ft) away from the previous site, and site 3 was 1.25 m (4.1 ft) downstream from site 2.



Figure 32.) Image of Site B during the B1 tracer study showing labeled flags and their relative positions to each other.

Two mini wells each 44.3 cm (17.44 in) long (Figure 33) were placed in the channel bed (well 1) and bank (well 2) between sites 1 and 2. Well 1 was 32.1 cm (12.64 in) exposed and well 2 was 31 cm (12.20 in) exposed. The wells have an opening of 0.7 cm (0.276 in) a closeup of which is shown in (Figure 34). The placement resulted in the opening of well 1 being approximately 8 cm deep and the opening of well 2 being approximately 9 cm deep. Figure 32 visually shows the positions of these sampling locations. In addition to the two mini well sampling locations, the surface water in a lateral cavity between sites 2 and 3 was sampled. It is expected that this lateral cavity is acting as a TSZ in addition to the channel bed and the channel bank subsurface.



Figure 33.) Mini wells inserted into the bank and streambed.



Figure 34.) Close up of the mini well opening that was approximately 0.7 cm long.

The B1 tracer study had a continuous injection of bromide that was started at 2:56 pm and lasted for 2.5 hours. Bromide was injected at 55 mL/min and was injected 0.9144 m (3 ft) upstream from the sampling location Site 1. The velocity of the stream was estimated to be 0.274 m/s (0.9 ft/s), however flow conditions were very low during this tracer study and measurements were difficult (Figure 35). The velocity was estimated by timing a pulse of Rhodamine dye in a short section of the channel because it was not possible to use the electromagnetic flow meter in the flow conditions.



Figure 35.) Different flow conditions at the start and end of B1.

A background sample was collected at each sampling site in the main channel and in the TSZs prior to injection. Additional surface water samples were taken at regular intervals after the start of injection and continued for 3.25 hours. Samples were collected after injection ended. Fewer samples were collected from the subsurface wells in the bank and channel at greater time intervals. Arrival of tracer concentrations in the subsurface was expected to take a longer amount of time.

Results from the B1 tracer study are shown in Figure 36. The injection plateau was higher than the site plateaus, suggesting that there was some lateral outflow. Based on the bank storage data points, it was concluded that it was not interacting substantially with the main channel flow and is not a significant storage zone under these hydrologic conditions. As a contrast, the other TSZs that were sampled showed observable concentrations of the bromide tracer and therefore underwent exchange with the main channel flow.

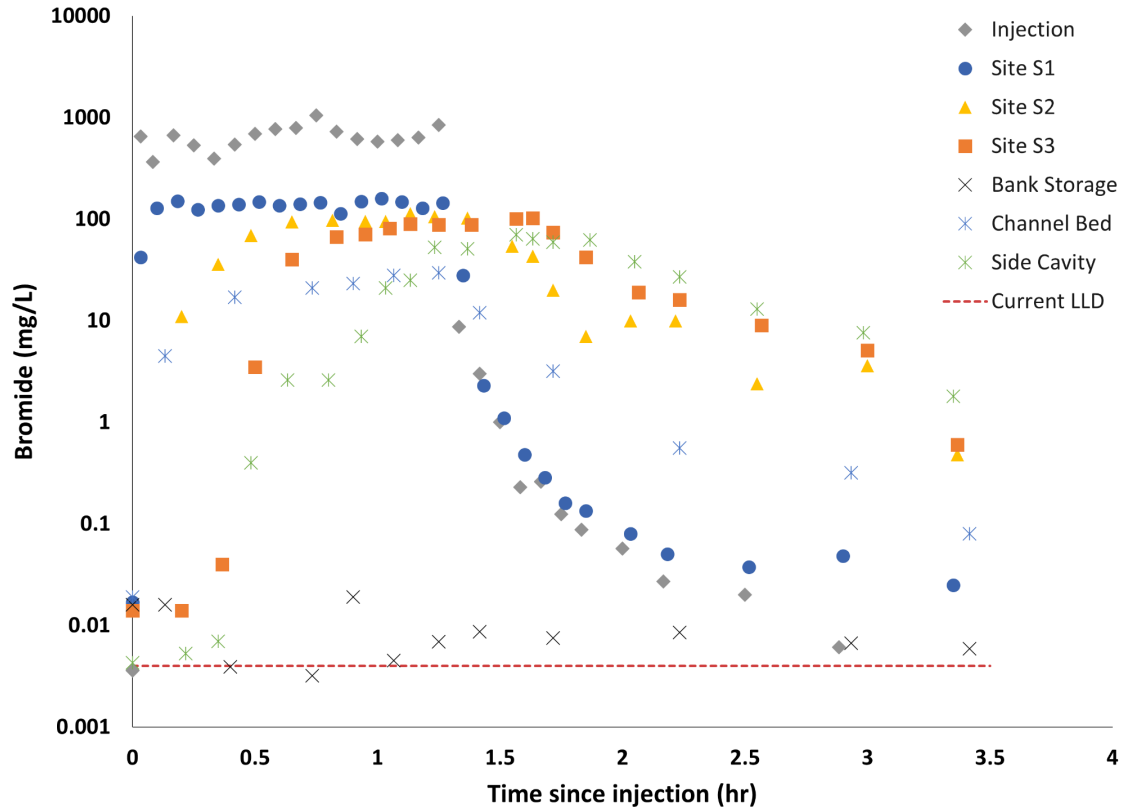


Figure 36.) Results from the B1 tracer of the injection, three main channel sites, and three potential TSZs.

Samples from tracers were processed with an ion chromatograph that had a lower detection limit (LLD) of 0.058 ppm and higher limit of 100 ppm. This LLD was based on 20 samples each of standards. These standards included 0.01ppm, 0.05ppm, 0.1ppm, and 0.25ppm that were processed by the IC. The LLD of 0.058ppm was calculated from the Type 2 error at a 5% significance level based on the 0.1ppm standards.

A second tracer injection began at Site B (B2) at 3:36pm and lasted 1.4 hours. The water level was much higher relative to the flow during the B1 experiment (Figure 37). Depths were 0.0762 m (0.25 ft), 0.091 m (0.3 ft), and 0.61 m (0.2 ft). The

stream velocities were measured at different locations in the stream. Measured velocities were 0.59 m/s (1.95 ft/s), 0.35 m/s (1.155 ft/s), and 0.18 m/s (0.6 ft/s). The stream discharge was an average of 0.031 m³/s (1.10 ft³/s).



Figure 37.) Flow conditions during B2.

The segment of stream used for the B2 tracer study was 32.9 m (108 ft) long. Due to higher flow, sampling from a longer reach was necessary for characterization of the hydrologic conditions. Surficial sampling sites were placed at distances of 6.1 m, 19.5 m, 32.9 m, or 20 ft, 64 ft, and 108 ft in US Customary, from the injection site. The injection site was moved upstream from where the injection

was placed for the B1 study. Surface sampling was completed at the same Sites 1 and 3 that were used in B1. The lateral cavity location was also re-used as a surface TSZ. The subsurface wells were placed in similar locations as the previous B1 study. Two additional surface water sampling locations (Site 4 and Site 5) were added further downstream in the main channel. (Site 2 from the B1 study was not used in the B2 study.) The bromide mixture was injected at 55 mL/min and was injected 6.1 m (20 ft) upstream from the first sampling site. The injectate had a target concentration of 200g/L while the bromide concentration was 6.5 mg/L once it mixed into Miller Run. The injection time for B2 was 1.4 hours but sample collection continued for a total of 4 hours. Samples were collected after injection ended. An overview of a portion of the sampling sites can be seen in Figure 38.



Figure 38.) Tracer setup, sampling locations marked by flags, and some transient storage zones.

The results from the B2 tracer are plotted in Figure 39. The plateaus of each site are fairly similar in magnitude, but the tails of the breakthrough curves are all different suggesting different sizes of storage areas and storage zone exchange rates. Some of the storage zones had very unique characteristics, such as the channel bed and bank storage, that were quite different from the main channel

characteristics. The bank storage points remained low as they did in the B1 study, implying that the exchange with the main channel flow was minimal.

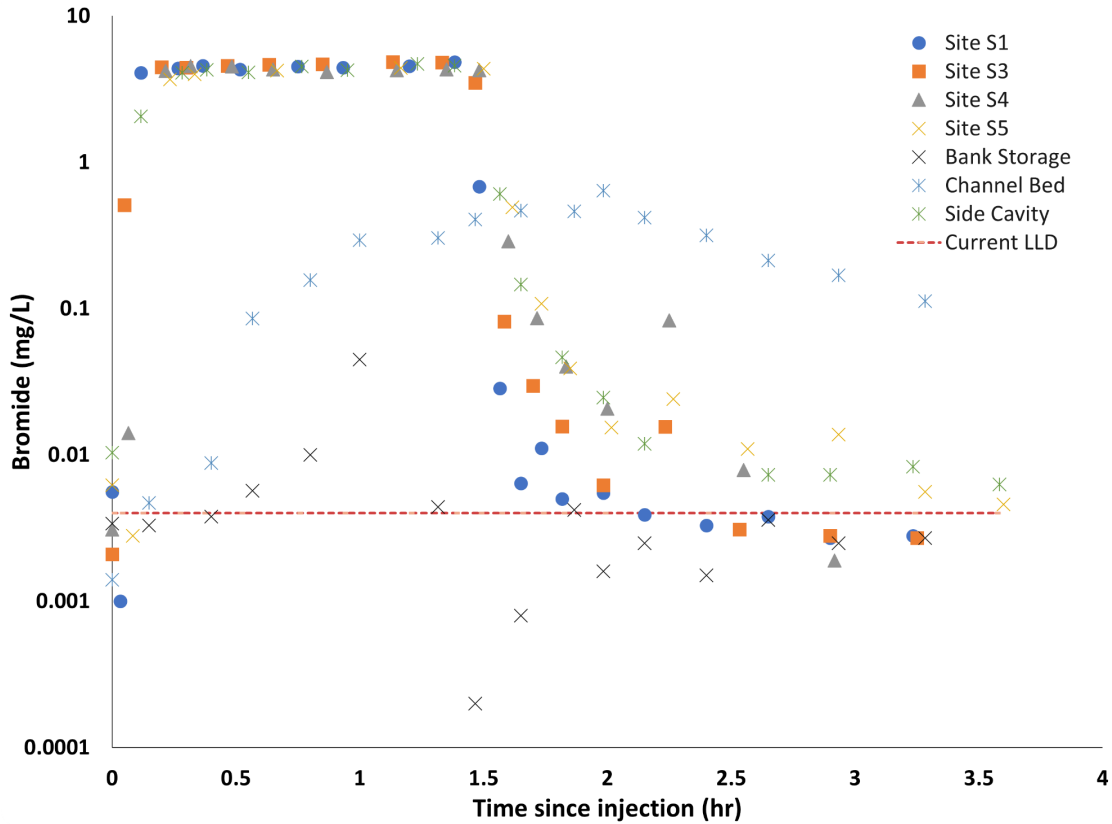


Figure 39.) Results from B2 from four main channel sampling sites and 3 potential TSZs.

Samples from tracers were processed with an ion chromatograph that had a lower detection limit (LLD) of 0.058 ppm and higher limit of 100 ppm. The LLD was the same as the samples were run on the same set up as B1.

Modeling Results

The OTIS-2Stor model was used to simulate the breakthrough curves that were observed during the B1 and B2 tracer studies. Use of the parameter estimation capabilities with NLS regression resulted in TSZ parameters (storage area and

exchange rate) that did not make sense when considering the physical characteristics of Site B on Miller Run. Therefore, a manual trial and error method was employed to fit the model simulation results to the observed data. Model variables, dispersion (D), discharge (Q), main channel cross sectional area (A), and lateral inflow and outflow were changed one by one within physically reasonable ranges. The dispersion coefficient was not easily estimated based on the collected data, and therefore other similar studies were consulted to determine the appropriate range (Wagner and Harvey, 1997; Stofleth and Shields, 2008; Tayfur, 2009).

B2 Transient Storage Zone Modeling

Best-fit model parameters were determined based on visual examination of graphs comparing the model simulation results and the observed data (see Appendix B). Because the OTIS-2Stor model is an executable that reads text files as input and output text files, a short script file was created in Matlab (see Appendix A) to assist in the process of trial and error model simulation. After many model iterations, the final best fit model simulations for the B2 tracer study are shown in Figures 40 through 44. Figure 40 shows the results from the injection site to the main channel surface water sampling site 1. Figure 41 compares the model and observed data from the main channel sampling site 3. Figure 42 compares the model and data from site 4 and Figure 43 compares the model and data from site 5. Figure 44 compares two TSZ results from the second reach between site 1 and site 3. This section is where the channel bed subsurface

TSZ was sampled and where the lateral cavity TSZ was sampled. In all cases, there is agreement between the observed data and the modeled results.

In the second reach in particular, the availability of TSZ observed data enabled a clearer process for fitting the model to the data. As mentioned in the methods section, the tail of the breakthrough curves contain the data that are influenced by the storage zone processes. However, as the concentrations get lower on the tail, it becomes harder to distinguish these values from background concentrations. While the surface water breakthrough curve tail has lower concentrations, the TSZ samples have higher concentrations. The fit of the model could be completed by examining how well the model simulated concentrations of bromide in the two TSZs.

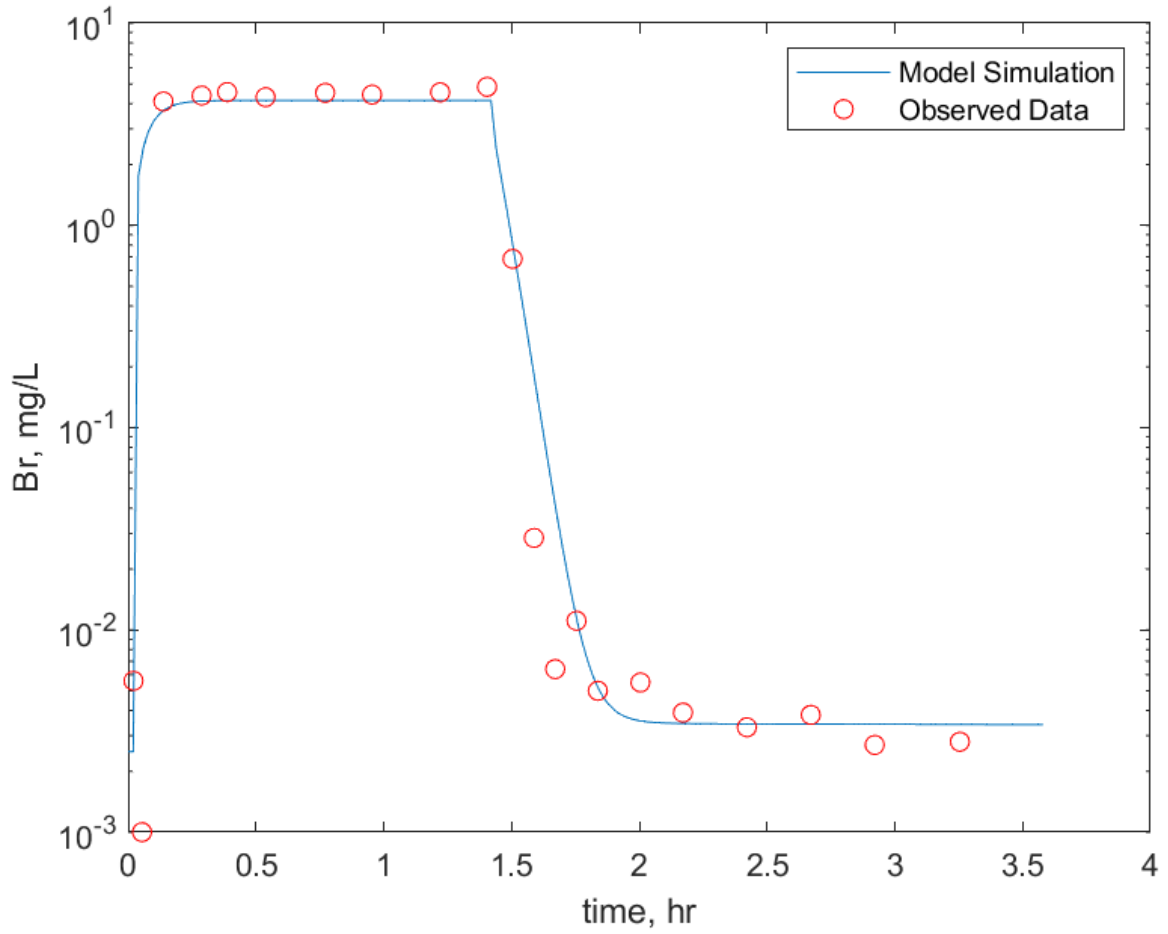


Figure 40.) Matlab-generated graph showing data collected from B2 Site 1 (red circles) and the best-fit OTIS-2Stor simulation.

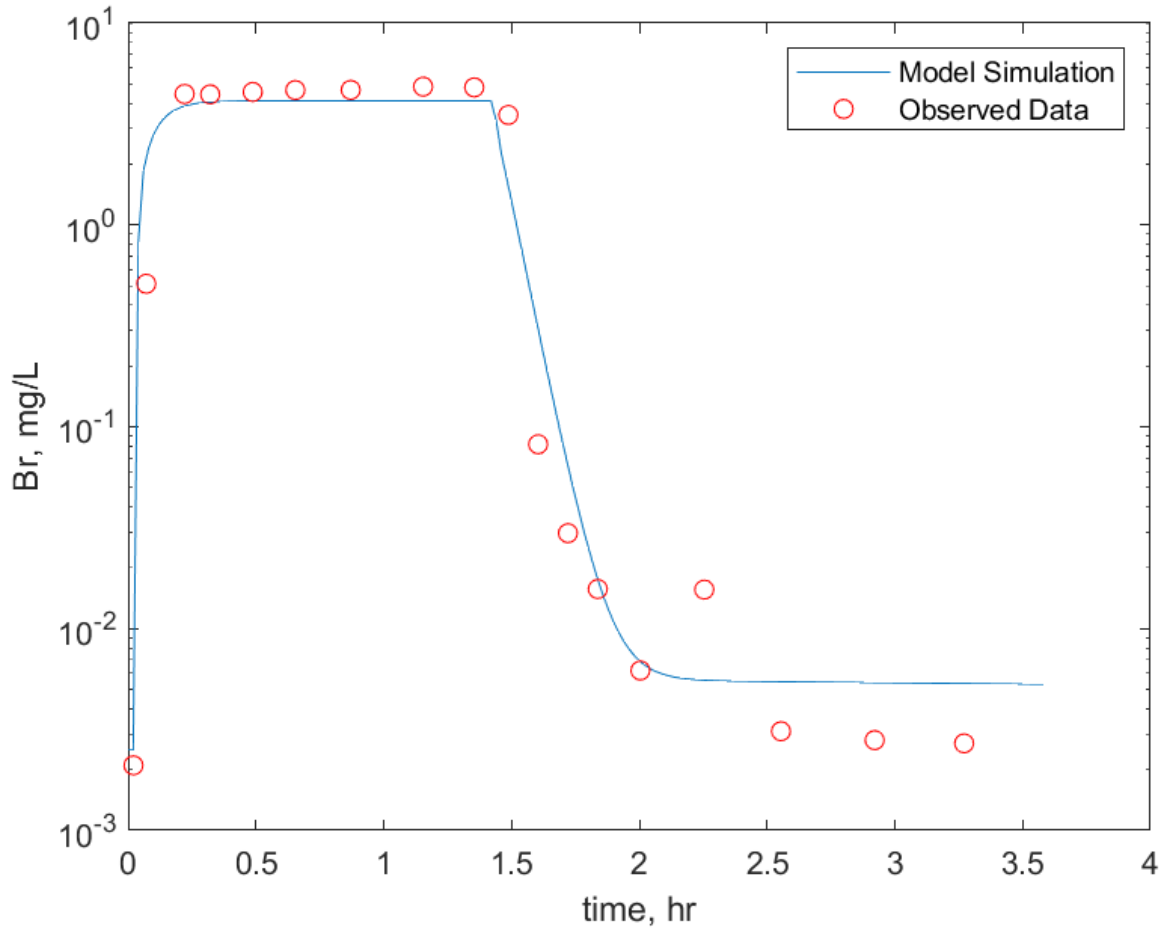


Figure 41.) B2 Site 3 data points shown as red circles and OTIS-2Stor resulting simulation that approximates the data.

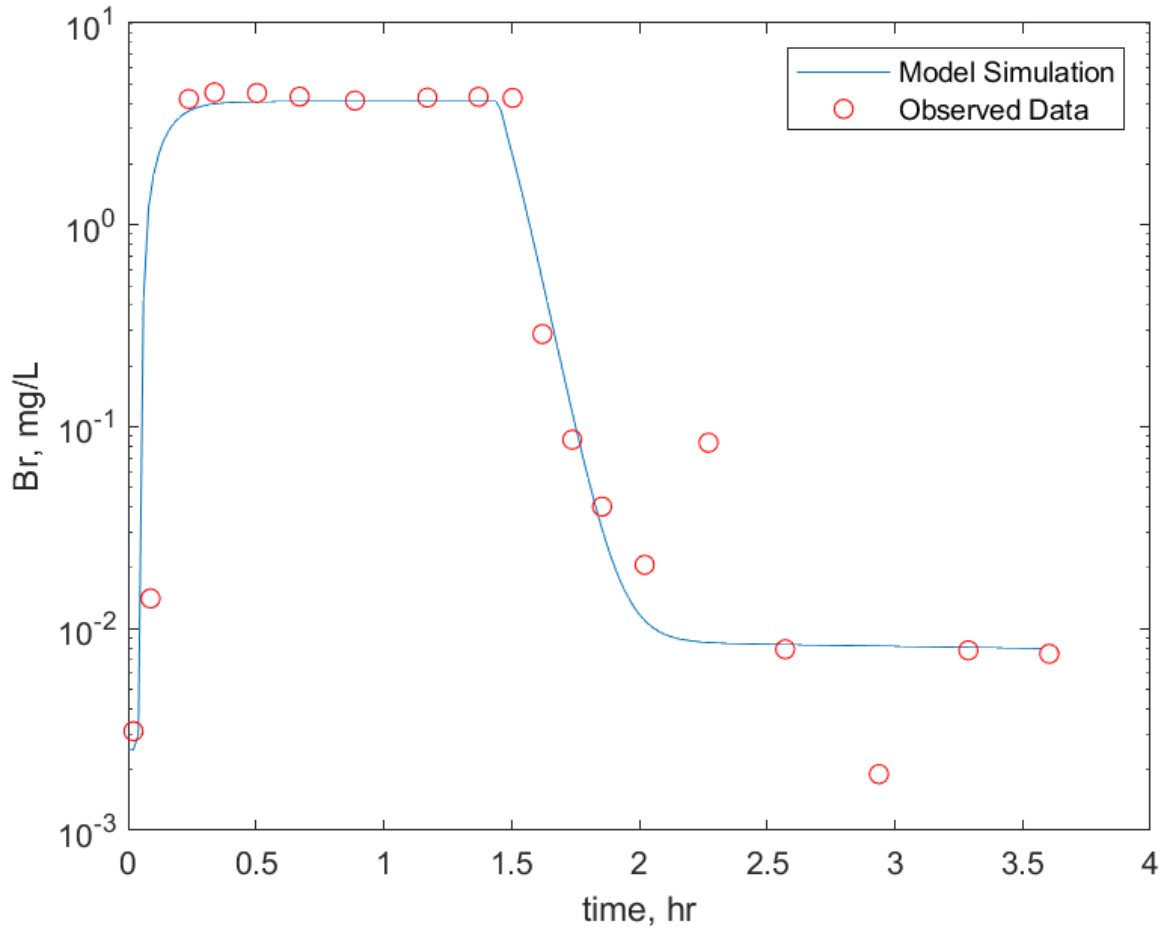


Figure 42.) B2 Site 4 observed data (red circles) with the modeled approximation using OTIS-2Stor.

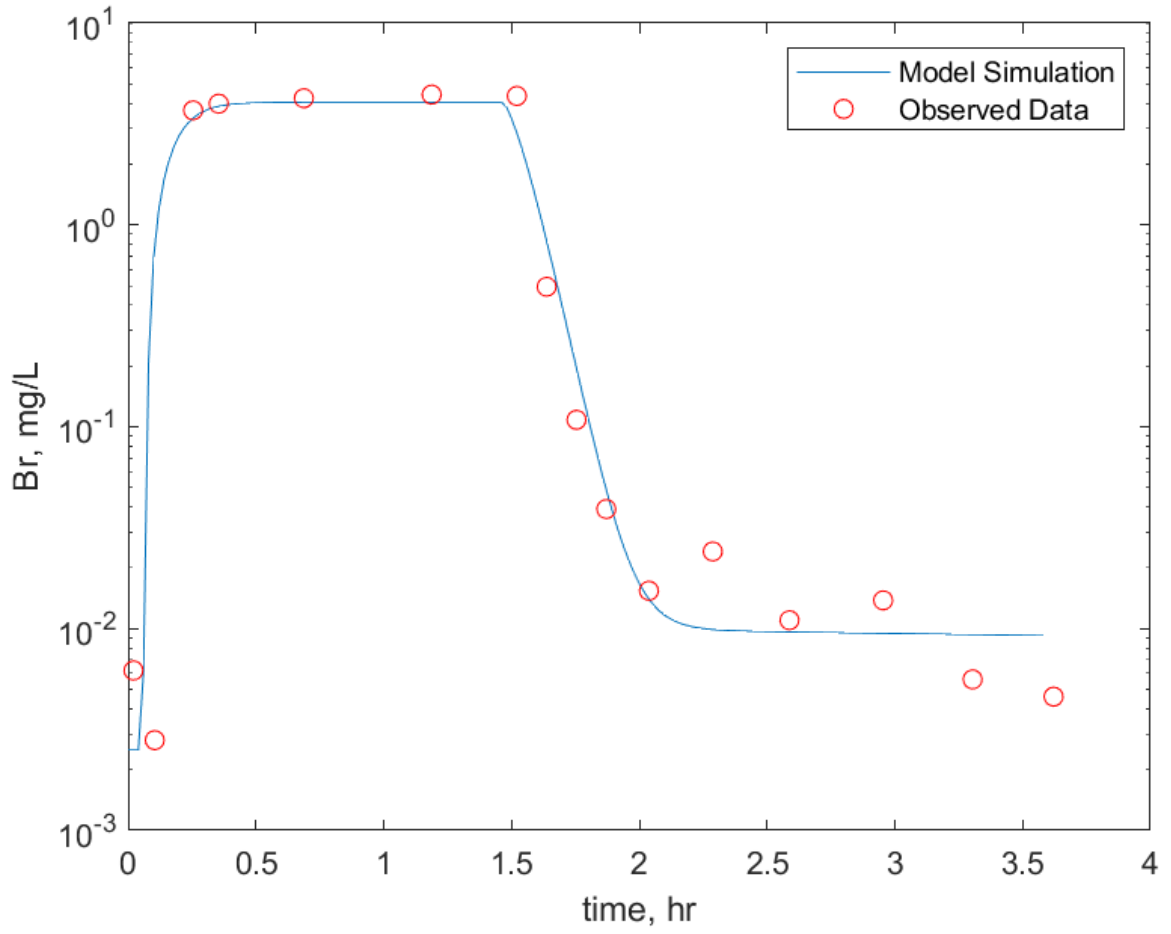


Figure 43.) Observed data from B2 Site 5 (red circles) and the OTIS-2Stor model simulation.

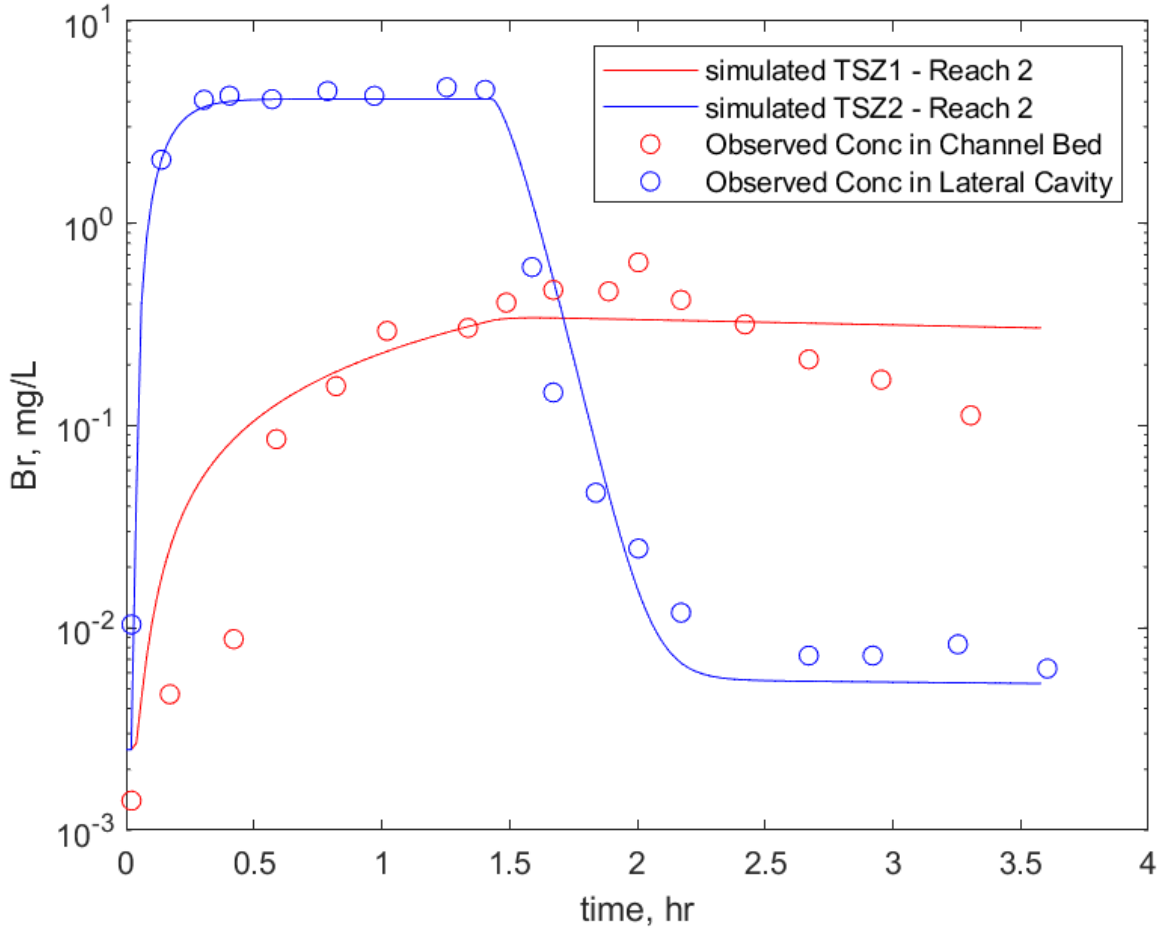


Figure 44.) Storage zone results from B2. The first TSZ is the stream’s channel bed (red circles - data, red line - OTIS-2Stor model simulation). The second TSZ is the lateral cavity (blue circles - data, blue line - OTIS-2Stor model simulation).

The final parameters used for the modeling results (Figure 40 - Figure 44) are consolidated into Table 3. The main channel area, storage zone areas, and storage zone exchange rates were used in Equation 4 to calculate the residence times in each storage zone.

$$t_{stor} = \frac{A_s}{\alpha A} \quad (4)$$

where

$$A_s = \text{Storage Zone Area [L}^2\text{]}$$

$$\alpha = \text{Storage Zone Exchange Coefficient [1/sec]}$$

$$A = \text{Main Channel Area [L}^2\text{]}$$

$$t_{stor} = \text{Residence Time of Storage Zones [sec]}$$

Storage zone 2 was much faster than storage zone 1. The difference between the lateral cavity (storage zone 2) and the channel bed (storage zone 1) is apparent in the large differences in residence times. The residence time of the lateral cavity ranged from 91 to 250 sec or 1.52 to 4.17 min with an average of 2.52 min. These values are slightly smaller than the mean residence times for similar lateral cavity environments from Table 1 (ranging from 4 to 35 minutes).

Conversely, the stream bed TSZ was much slower than the lateral cavity TSZ. The residence times were on the scale of hours rather than seconds or minutes. The values ranged from 13 to 46 hours with an average of 27 hours. These residence times compare well with the previous studies on streambed sediment TSZs cited in Table 1. This longer residence time also helps to explain why the observed tracer concentration in the channel bed TSZ did not start decreasing during the approximately 4 hour sampling time period of the tracer study.

Table 3.) Parameters that were calculated by OTIS or held as a constant.

Parameters	Reach 1	Reach 2	Reach 3	Reach 4
Storage zone 1 cross-sectional area (m ²)	0.929	0.604	0.302	0.622
Storage zone 1 exchange coefficient (/sec)	1.5e-4	2.8e-4	8.5e-5	1.0e-4
Storage zone 2 cross-sectional area (m ²)	0.116	0.0836	0.0464	0.0464
Storage zone 2 exchange coefficient (/sec)	2.5e-2	9e-3	4.5e-3	1e-2
Lateral inflow rate (m ³ /sec-m)	4.2e-3	0.00	0.00	0.00
Lateral outflow rate (m ³ /sec-m)	1.7e-4	4.8e-6	4.8e-6	4.8e-6
Main channel area (m ²)	0.0372	0.0372	0.0743	0.0511
Storage zone 1 residence time	1.67e+5 (sec) 2783 (min) 46 (hour)	5.80e+4 (sec) 967 (min) 16 (hour)	4.78e+4 (sec) 797 (min) 13 (hour)	1.22e+5 (sec) 2033 (min) 34 (hour)
Storage zone 2 residence time	125 (sec) 2.08 (min)	250 (sec) 4.17(min)	139 (sec) 2.32 (min)	90.9 (sec) 1.52 (min)

B1 Transient Storage Zone Modeling

While model simulation of the B2 tracer study proved challenging due to the likely losing stream hydrologic conditions in the fall 2022 that followed a very dry

summer 2022, the B1 tracer study was more difficult. As shown in Figure 35, the discharge rate in the channel was not constant for the duration of the tracer study. Lateral outflows were likely relatively large as well. Within the numerical solution of the advection-dispersion with inflow and storage equation, the time computation step became very small to ensure a stable solution. Trial and error parameter determination resulted in some of the observed conditions able to be simulated, however large portions of the tail observations were not well simulated with the model (Figure 45 and Appendix C). Without successful simulation of reach 1, the downstream reaches could not be simulated. Applying OTIS-2Stor with steady flow conditions was not effective. It is possible that a TSM could still be used with unsteady flow, or another modeling approach (Boano et al., 2014) might be more successful.

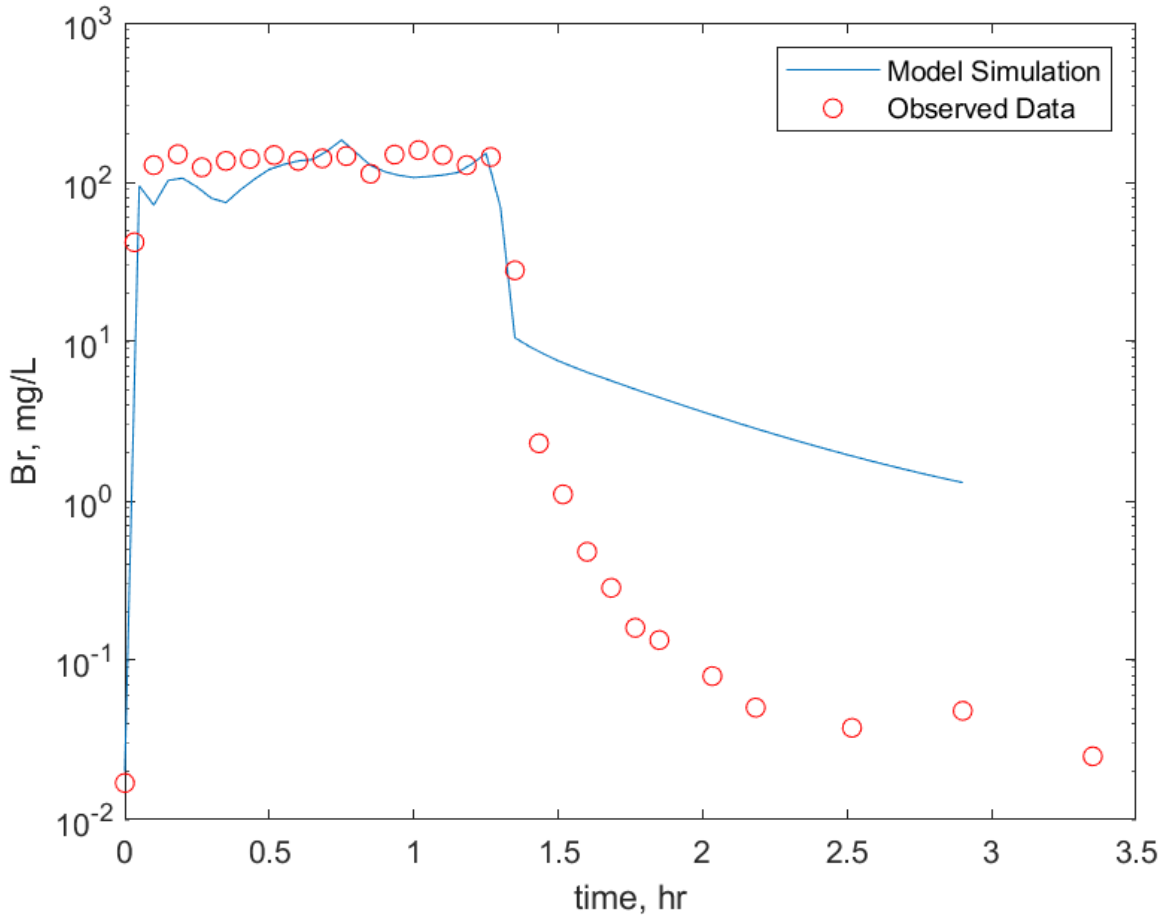


Figure 45.) Attempt to model the observed breakthrough curve of bromide at the main channel sampling site 1 during the B1 tracer study.

Conclusions

Based on the detailed site characterization, the three chosen sites for this study would provide appropriate variety for continued tracer studies in the future.

There would be potential to compare TSZ processes in the different types of storage zones that are present at the 3 sites. It is important to continue tracer studies in a variety of hydrologic conditions as well as in a variety of physical conditions as identified in the initial study Sites A, B, and C. Flow conditions (and

potentially water table conditions) vary dramatically depending on the time of year and tracer studies done under differing conditions would contribute to an improved understanding of the hydrologic conditions of Miller Run.

Tracer Study and Modeling Results

Looking only at the trends in the breakthrough curves for tracer studies B1 and B2, it is clear that the rate of exchange for a given TSZ may be different depending on the flow conditions. In Figure 36, the bromide concentrations in the channel bed sediment TSZ increase more quickly than the lateral cavity TSZ as the plateau tracer concentration is reached for the B1 tracer study. This is also true on the tail of the breakthrough curves where the channel bed sediment TSZ decreases more quickly than the side channel TSZ. In Figure 39, the bromide concentration in the lateral cavity TSZ rises quite quickly and at a similar rate to the surface sampling sites in the main channel for the B2 tracer study. In contrast, the tracer concentration in the channel bed sediment TSZ rises slowly and does not start to decrease within the data collection time. Because the TSZ samples were taken in approximately the same locations during both tracer studies, these two results highlight the need for repeated tracer studies in different hydrologic conditions to fully understand the processes in TSZs.

The B2 tracer study resulted in model simulation that allowed for the estimation of hydrologic residence times in the TSZs. The residence times between the fast and slow storage zones were very distinctive from each other. Calculated residence times for the lateral cavity tended to be slightly lower than the mean

times found in Table 1, but that could potentially be due to the smaller nature of Miller Run compared to the streams used in the studies cited in Table 1.

Similarly, the streambed sediment residence times agreed well with the residence times listed for similar TSZ environments in Table 1. Also during modeling with OTIS-2Stor, samples taken directly from identified TSZs were essential for modeling simulation success. Difficulties when creating models due to problems fitting both breakthrough curves and breakthrough curve tails were able to be resolved using observed tracer concentration values from the TSZs. Two particular TSZs, the streambed and lateral cavity, were used to create improved model simulations that best fit the TSZs known bromide concentrations using parameters that made physical sense.

Geophysical Methods for Understanding Subsurface TSZs

While the intended purpose of the GPR, which was to attempt to find the water table, was not successful, a possible explanation would be that it was simply too deep for the 500 MHz antennas to penetrate. A revisit using a lower signal frequency might be able to reach a lower depth because water tables under losing streams could potentially be quite deep. It would also be worth running GPR lines close to the channel incision of Miller Run after sampling site 3 at study Site B to determine if there is an underlying cause that could be due to subsurface structure.

There is also a possibility that ER may still work with a different configuration, different tracers, or a combination that would be dependent on the background

conductivity. There was also some difficulty with the channel cross section shape, such as the heavily incised banks at Site B for example, which could contribute another obstacle preventing ER from being useful for additional data collection during tracer studies.

Combining Tracer Study and Geophysical Data Findings

Based on the unsuccessful water table interface using GPR, the attempted model simulation of tracer study B1 where lateral outflow was essential to a successful fit, and the active lowering of the water level during the B1 tracer study, it is strongly suggested that Miller Run and its tributary were losing streams when these measurements and studies were being collected or performed. The geophysical data were collected in the spring 2022 and the tracer studies were performed in the fall of 2022. In order to properly handle model simulation of a losing stream, it would require the application of an unsteady flow model or potentially any alternative approach to simulating TSZ processes in streams.

Bibliography

- Adagunodo, T. A., & Sunmonu, L. A. (2013). The study of basement pattern of an industrial estate. LAMBERR Academic Publishing.
- Adagunodo, T. A., Akinloye, M. K., Sunmonu, L. A., Aizebeokhai, A. P., Oyeyemi, K. D., & Abodunrin, F. O. (2018). Groundwater exploration in Aaba residential area of Akure, Nigeria. *Frontiers in Earth Science*, 6, 66.
- Akhtar, N., Syakir, M. I., Anees, M. T., Qadir, A., & Yusuff, M. S. (2021). Characteristics and Assessment of Groundwater. *Groundwater Management and Resources*, 3.
- Alley, W. M., Reilly, T. E., & Franke, O. L. (1999). Sustainability of ground-water resources (Vol. 1186). US Department of the Interior, US Geological Survey.
- Bencala, K. E., Gooseff, M. N., & Kimball, B. A. (2011). Rethinking hyporheic flow and transient storage to advance understanding of stream-catchment connections. *Water Resources Research*, 47(3).
- Boano, F., Harvey, J. W., Marion, A., Packman, A. I., Revelli, R., Ridolfi, L., & Wörman, A. (2014). Hyporheic flow and transport processes: Mechanisms, models, and biogeochemical implications. *Reviews of Geophysics*, 52(4), 603-679.
- Böhlke, J. K., Antweiler, R. C., Harvey, J. W., Laursen, A. E., Smith, L. K., Smith, R. L., & Voytek, M. A. (2009). Multi-scale measurements and modeling of denitrification in streams with varying flow and nitrate concentration in the upper Mississippi River basin, USA. *Biogeochemistry*, 93, 117-141.
- Breden, C. (2012). Water Quality and Hydrologic Monitoring and Modeling of Miller Run.
- Brenner, F. J., Steiner, R. P., & Mondok, J. J. (1996). Groundwater-surface water interaction in an agricultural watershed. *Journal of the Pennsylvania Academy of Science*, 3-8.
- Bruckner, Monica Z. (2021). "Hydrological Tracers." Carleton University. https://serc.carleton.edu/microbelife/research_methods/environ_sampling/hydrotrace.html.
- Burger, H. R., Burger, D. C., & Burger, H. R. (1992). Exploration geophysics of the shallow subsurface (Vol. 8). New Jersey: Prentice Hall.
- Burke, M. (2009). Characterization of Miller Run and Conceptual Plan for Watershed Restoration. Bucknell University, Lewisburg, PA.
- Castro, N. M., & Hornberger, G. M. (1991). Surface-subsurface water interactions in an alluviated mountain stream channel. *Water Resources Research*, 27(7), 1613-1621.

- Chen, X. (2011, May). Fluctuation of hyporheic zone thickness due to inflow and outflow across the water-sediment interface. In 2011 International Symposium on Water Resource and Environmental Protection (Vol. 1, pp. 388-391). IEEE.
- Chesapeake Conservancy (2019). Union County Forest Buffer Summary 100 ft. Width.
https://cicwebresources.blob.core.windows.net/enhancedflowpaths/pa_downloader/county/Buffer100ft/BufferReports100/Union_Buffer_Summary100.pdf.
- Choi, J. Y. (1998). Transport modeling of metal contaminants in a stream-aquifer system (Doctoral dissertation, The University of Arizona).
- Choi, J., Harvey, J. W., & Conklin, M. H. (2000). Characterizing multiple timescales of stream and storage zone interaction that affect solute fate and transport in streams. *Water Resources Research*, 36(6), 1511-1518.
- Donaldson, J.R. and Tryon, P.V. (1990). User's guide to STARPAC – The standards, time-series, and regression package: National Institute of Standards and Technology Internal Report NBSIR 86-3448.
- Giambastiani, Y., Errico, A., Preti, F., Guastini, E., & Censini, G. (2022). Indirect root distribution characterization using electrical resistivity tomography in different soil conditions. *Urban Forestry & Urban Greening*, 67, 127442.
- “Google Earth.” Accessed February 18, 2022.
<https://earth.google.com/web/@40.94715957,-76.88909441,153.21925484a,517.83183891d,35y,oh,ot,or>.
- Gooseff, M. N., Hall Jr, R. O., & Tank, J. L. (2007). Relating transient storage to channel complexity in streams of varying land use in Jackson Hole, Wyoming. *Water Resources Research*, 43(1).
- Harvey, J. W., & Fuller, C. C. (1998). Effect of enhanced manganese oxidation in the hyporheic zone on basin-scale geochemical mass balance. *Water Resources Research*, 34(4), 623-636.
- Harvey, J. W., & Wagner, B. J. (2000). Quantifying hydrologic interactions between streams and their subsurface hyporheic zones.
- Harvey, J. W., Wagner, B. J., & Bencala, K. E. (1996). Evaluating the reliability of the stream tracer approach to characterize stream-subsurface water exchange. *Water resources research*, 32(8), 2441-2451.
- Harvey, J. W., Newlin, J. T., & Krupa, S. L. (2006). Modeling decadal timescale interactions between surface water and ground water in the central Everglades, Florida, USA. *Journal of Hydrology*, 320(3-4), 400-420.
- Harvey, J. W., Saiers, J. E., & Newlin, J. T. (2005). Solute transport and storage mechanisms in wetlands of the Everglades, south Florida. *Water Resources Research*, 41(5).

- Herrman, K. S., Bouchard, V., Granata, T., Carey, A. E., & Moore, R. H. (2010). The effect of riparian land use on transport hydraulics in agricultural headwater streams located in northeast Ohio, USA. *Hydrological Processes: An International Journal*, 24(1), 1-12.
- Hester, E. T., & Fox, G. A. (2020). Preferential flow in riparian groundwater: Gateways for watershed solute transport and implications for water quality management. *Water Resources Research*, 56(12), e2020WR028186.
- Jackson, T. R., Haggerty, R., Apte, S. V., Coleman, A., & Drost, K. J. (2012). Defining and measuring the mean residence time of lateral surface transient storage zones in small streams. *Water Resources Research*, 48(10).
- Jones, J. B., & Mulholland, P. J. (1999). *Streams and ground waters*. Elsevier.
- Kilpatrick, F. A., & Cobb, E. D. (1985). Measurement of discharge using tracers (p. 52). Washington, DC, USA: Department of the Interior, US Geological Survey.
- Kim, B. K., Jackman, A. P., & Triska, F. J. (1990). Modeling transient storage and nitrate uptake kinetics in a flume containing a natural periphyton community. *Water Resources Research*, 26(3), 505-515.
- Manu, E., Preko, K., & Wemegah, D. D. (2014). Estimation of water table depths and local groundwater flow pattern using the Ground Penetrating Radar. *International Journal of Scientific and Research Publications*, 4(8), 1-12.
- Milsom, J. (2003). *Field geophysics* (Vol. 25). John Wiley and Sons.
- Noh, H., Kwon, S., Seo, I. W., Baek, D., & Jung, S. H. (2020). Multi-gene genetic programming regression model for prediction of transient storage model parameters in natural rivers. *Water*, 13(1), 76.
- O'Connor, B. L., Hondzo, M., & Harvey, J. W. (2010). Predictive modeling of transient storage and nutrient uptake: Implications for stream restoration. *Journal of Hydraulic Engineering*, 136(12), 1018-1032.
- Oenema, O., van Liere, L., & Schoumans, O. (2005). Effects of lowering nitrogen and phosphorus surpluses in agriculture on the quality of groundwater and surface water in the Netherlands. *Journal of Hydrology*, 304(1-4), 289-301.
- Runkel, R. L. (1998). One-dimensional transport with inflow and storage (OTIS): A solute transport model for streams and rivers (Vol. 98, No. 4018). US Department of the Interior, US Geological Survey.
- "OTIS Documentation: User's Guide to STARPAC." Accessed April 14, 2023. <https://water.usgs.gov/software/OTIS/addl/starpac/nls.html#ch1>.
- Packman, A. I., & Bencala, K. E. (2000). Modeling surface-subsurface hydrological interactions.

- Piscart, C., Navel, S., Maazouzi, C., Montuelle, B., Cornut, J., Mermillod-Blondin, F., ... & Marmonier, P. (2011). Leaf litter recycling in benthic and hyporheic layers in agricultural streams with different types of land use. *Science of the Total Environment*, 409(20), 4373-4380.
- Rantz, S. E. (1982). *Measurement and computation of streamflow* (Vol. 2175). US Department of the Interior, Geological Survey.
- Runkel, R. L. (1998). One-dimensional transport with inflow and storage (OTIS): A solute transport model for streams and rivers (Vol. 98, No. 4018). US Department of the Interior, US Geological Survey.
- Runkel, R. L. (2000). Using OTIS to model solute transport in streams and rivers. US Department of the Interior, US Geological Survey.
- Salam, M. A., Rahman, Q. M., Ang, S. P., & Wen, F. (2017). Soil resistivity and ground resistance for dry and wet soil. *Journal of Modern Power Systems and Clean Energy*, 5(2), 290-297.
- Schaffer, A. C. (2008). Hydrologic and Water Quality Assessment of Miller Run: A Study of Bucknell University's Impact.
- Shook, C. L., Ketchen Jr, D. J., Hult, G. T. M., & Kacmar, K. M. (2004). An assessment of the use of structural equation modeling in strategic management research. *Strategic management journal*, 25(4), 397-404.
- Sobota, D. J., Johnson, S. L., Gregory, S. V., & Ashkenas, L. R. (2012). A stable isotope tracer study of the influences of adjacent land use and riparian condition on fates of nitrate in streams. *Ecosystems*, 15, 1-17.
- Stofleth, J. M., Shields Jr, F. D., & Fox, G. A. (2008). Hyporheic and total transient storage in small, sand-bed streams. *Hydrological Processes: An International Journal*, 22(12), 1885-1894.
- Tayfur, G. (2009). GA-optimized model predicts dispersion coefficient in natural channels. *Hydrology Research*, 40(1), 65-78.
- "The Quality of the Nation's Groundwater | U.S. Geological Survey." Accessed February 15, 2022.
<https://www.usgs.gov/news/featured-story/quality-nations-groundwater>.
- Triska, F. J., Duff, J. H., & Avanzino, R. J. (1993). The role of water exchange between a stream channel and its hyporheic zone in nitrogen cycling at the terrestrial-aquatic interface. *Hydrobiologia*, 251, 167-184.
- Union County. "UNION COUNTY, PA Part II Comprehensive Plan Elements," n.d.
- Wagner, B. J., & Harvey, J. W. (1997). Experimental design for estimating parameters of rate-limited mass transfer: Analysis of stream tracer studies. *Water Resources Research*, 33(7), 1731-1741.

- Ward, A. S., Gooseff, M. N., & Singha, K. (2010). Characterizing hyporheic transport processes—Interpretation of electrical geophysical data in coupled stream–hyporheic zone systems during solute tracer studies. *Advances in Water Resources*, 33(11), 1320-1330.
- Ward, A. S., Gooseff, M. N., & Singha, K. (2010). Imaging hyporheic zone solute transport using electrical resistivity. *Hydrological Processes: An International Journal*, 24(7), 948-953. <https://doi.org/10.1002/HYP.7672>.
- “Water Quality for Agriculture.” Accessed February 15, 2022. <https://www.fao.org/3/t0234e/t0234e01.htm>.
- “Web Soil Survey - Home.” Accessed April 13, 2023. <https://websoilsurvey.nrcs.usda.gov/app/>.
- Winter, T. C., J.W. Harvey. (2000). *Ground water and surface water: a single resource*. Diane Publishing.
- Wondzell, S. M. (2011). The role of the hyporheic zone across stream networks. *Hydrological Processes*, 25(22), 3525-3532.
- Wroblicky, G. J., Campana, M. E., Valett, H. M., & Dahm, C. N. (1998). Seasonal variation in surface-subsurface water exchange and lateral hyporheic area of two stream-aquifer systems. *Water Resources Research*, 34(3), 317-328.
- Yochum, S. E., & Reynolds, L. V. (2018). *Guidance for stream restoration*. US Department of Agriculture, Forest Service, National Stream & Aquatic Ecology Center.
- Zarnetske, J. P., Haggerty, R., Wondzell, S. M., & Baker, M. A. (2011). Dynamics of nitrate production and removal as a function of residence time in the hyporheic zone. *Journal of Geophysical Research: Biogeosciences*, 116(G1).

Appendix A - Matlab Code to Run OTIS-2Stor and Plot Results

Matlab code to run the OTIS-2Stor executable file and plot [results](#)

The observed breakthrough curve data is loaded into Matlab, followed by running the OTIS-2Stor executable with the input files that are co-located in the folder with the executable file. The executable created an output file that contains the model simulated solute concentrations. Matlab code was created to read this file. Finally, plots that compare the observed breakthrough curves to the modeled curve are created.

The OTIS-2Stor executable can be run with parameter estimation enabled and without it enabled.

Import Observation Data.....	1
Run OTIS2StorComb.exe	1
Import Solute Results from text file.	1
Initialize variables.	2
Format for each line of text:.....	2
Open the text file.....	2
Read columns of data according to the format.....	2
Close the text file.....	2
Post processing for unimportable data.	2
Create output variable	3
Clear temporary variables	3
Plots for each sampling collection site	3

Read columns of data according to the format.

This call is based on the structure of the file used to generate this code. If an error occurs for a different file, try regenerating the code from the Import Tool.

```
dataArray = textscan(fileID, formatSpec, 'Delimiter', ',', 'WhiteSpace', '', 'TextType', 'string', 'ReturnOnError', false);
```

Close the text file.

```
fclose(fileID);
```

Post processing for unimportable data.

No unimportable data rules were applied during the import, so no post processing code is included. To generate code which works for unimportable data, select unimportable cells in a [file](#) and regenerate the script.

Create output [variable](#)

```
solute = [dataArray{1:end-1}];
```

Clear temporary variables

```
clearvars filename formatSpec fileID dataArray ans;
```

Plots for each sampling collection site

```
figure(1)
title('Site S1')
semilogy(solute(:,1),solute(:,2));
hold on
semilogy(B2S1Data(:,1),B2S1Data(:,2),'ro');
xlabel('time, hr')
ylabel('Br, mg/L')
legend('Model Simulation','Observed Data')
```

```
figure(2)
title('Site S3')
semilogy(solute(:,1),solute(:,3));
hold on
semilogy(B2S3Data(:,1),B2S3Data(:,2),'ro');
xlabel('time, hr')
ylabel('Br, mg/L')
legend('Model Simulation','Observed Data')
```



```

figure(3)
title('Site S4')
semilogy(solute(:,1),solute(:,4));
hold on
%semilogy(solute(:,1),previousS4)
semilogy(B2S4Data(:,1),B2S4Data(:,2),'ro');
xlabel('time, hr')
ylabel('Br, mg/L')
legend('Model Simulation','Observed Data')

```

```

figure(4)
title('Site S5')
semilogy(solute(:,1),solute(:,5));
hold on
%semilogy(solute(:,1),previousS5)
semilogy(B2S5Data(:,1),B2S5Data(:,2),'ro');
xlabel('time, hr')
ylabel('Br, mg/L')
legend('Model Simulation','Observed Data')

```

```

figure(5)
title('Storage Zones')
semilogy(solute(:,1),solute(:,7),'r-');
hold on
semilogy(solute(:,1),solute(:,11),'b-');
semilogy(B2ChBedData(:,1),B2ChBedData(:,2),'ro');
semilogy(B2CavData(:,1),B2CavData(:,2),'bo');
xlabel('time, hr')

```

```

ylabel('Br, mg/L')
legend('simulated TSZ1 - Reach 2','simulated TSZ2 - Reach 2','Observed Conc in Channel Bed','Observed Conc in Lateral Cavity')

```

Published with MATLAB® R2022a

Appendix B - OTIS-2Stor Input and Output Files for B2 Tracer Study

Control.inp

```
#####  
#####  
#  
#           OTIS-P control file  
#  
#  
# line      name of the:  
# ----      -  
# 1         parameter file  
# 2         flow file  
# 3         data file  
# 4         STARPAC input file  
# 5         parameter output file  
# 6         STARPAC output file  
# 7         solute output file  
# 8         sorption output file (ISORB=1 only)  
#  
#####  
#####  
O  
params.inp  
q.inp  
#data.inp  
#star.inp  
#params.out  
#star.out  
solute.out
```

Params.inp

```
#####  
#####  
#  
#           OTIS parameter file  
#  
#  
# Tracer Study Miller Run  
# Site B (2nd Study) Fall 2022  
#  
#####  
#####
```

Miller Run - Tracer B2

```
2      |  PRTOPT
0.02   |  PSTEP [hour]
2.0e-4 |  TSTEP [hour]
00.00  |  TSTART [hour]
3.567  |  TFINAL [hour]
0.0    |  XSTART [L]
0.0    |  DSBOUND [(L/sec)CU]
4      |  NREACH
2      |  NSTOR
#####
#####
#
# Physical Parameters
#
#       for I = 1, NREACH
#
#NSEG RCHLEN  DISP  AREAS1  ALPHA1  AREAS2  ALPHA2
# |   |   |   |   |   |   |
#####
#####
92 46.0  2.00  10  1.5e-4  1.25  2.5e-2
40 20.0  2.00  6.5  2.8e-4  0.90  9e-3
88 44.0  2.00  3.25  8.5e-5  0.50  4.5e-3
216 108.0  2.00  6.7  1.0e-4  0.50  1e-2
#####
#####
#
# Number of Solutes and flags for decay and sorption
#
# NSOLUTE (col.1-5) IDECAY(col.6-10) ISORB(col.11-15)
#
# | |
#####
1 0 0
#####
#
# Decay Coefficients (IDECAY=1, only)
#
#       for I = 1, NREACH
#
#LAMBDA  LAMBDA2
# |
#####
#####
# Print Information
#####
4 0      NPRINT (col.1-5) IOPT (col.6-10)
46.0
```

```

66.0      (PRTLOC for I = 1, NPRINT)
110.0
164.0
#####
#
# Boundary Conditions
#
#####
4 1      NBOUND (col.1-5) IBOUND (col.6-10)
#####
#      for I = 1,NBOUND
#
#USTIME   USBC (for i=1,NSOLUTE)
#      |      |      |
#####
0.0      0.0025
0.021    6.5
1.421    0.0025
3.60     0.0025

Q.inp
#####
#####
#
#      OTIS steady flow file
#
# Miller Run - B2 Tracer Study (Fall 2022)
#
#####
#####
0.00     QSTEP [hour]
0.45     QSTART [L^3/second]
#####
#      for I = 1, NREACH
#
#QLATIN   QLATOUT   AREA   (CLATIN J=1,NSOLUTE)
#      |      |      |      |
#####
4.2e-3   5.9e-3   0.40   0.0025
0.00     1.7e-4   0.40   0.0025
0.00     1.7e-4   0.80   0.0025
0.00     1.7e-4   0.55   0.0025

```

Appendix C - OTIS-2Stor Input and Output Files for B1 Tracer Study

Control.inp

```
#####  
#####  
#  
#          OTIS-P control file  
#  
#  
# line      name of the:  
# ----      -  
# 1         parameter file  
# 2         flow file  
# 3         data file  
# 4         STARPAC input file  
# 5         parameter output file  
# 6         STARPAC output file  
# 7         solute output file  
# 8         sorption output file (ISORB=1 only)  
#  
#####  
#####  
O  
params.inp  
q.inp  
#data.inp  
#star.inp  
#params.out  
#star.out  
solute.out
```

Params.inp

```
#####  
#####  
#  
#          OTIS parameter file  
#  
# Tracer Study Miller Run  
# Site B1 (1st Study) Fall 2022  
#  
#####  
#####  
Miller Run - Tracer B2  
2      |  PRTOPT  
0.05   |  PSTEP [hour]  
1.0e-7 |  TSTEP [hour]
```

```

0.0    |   TSTART [hour]
2.883  |   TFINAL [hour]
0.0    |   XSTART [L]
0.0    |   DSBOUND [(L/sec)CU]
3      |   NREACH
2      |   NSTOR
#####
#
# Physical Parameters
#
#       for I = 1, NREACH
#
#NSEG RCHLEN   DISP   AREAS1   ALPHA1   AREAS2   ALPHA2
# |   |   |   |   |   |
#####
3 3.00   0.40   10.    2.e-2   5.0     3.65e-5
6 5.7    0.35   0.50   5.e-5   999     0
8 8.0    0.35   0.50   5.e-5   999     0
#####
#
# Number of Solutes and flags for decay and sorption
#
# NSOLUTE (col.1-5) IDECAY(col.6-10) ISORB(col.11-15)
#
# | |
#####
1 0 0
#####
#
# Decay Coefficients (IDECAY=1, only)
#
#       for I = 1, NREACH
#
#LAMBDA   LAMBDA2
# |
#####
#####
# Print Information
#####
3 0      NPRINT (col.1-5) IOPT (col.6-10)
3.0      (PRTLOC for I = 1, NPRINT)
9.0
13.0
#####
#
# Boundary Conditions
#
#####
28 3      NBOUND (col.1-5) IBOUND (col.6-10)

```

```

#####
#       for I = 1,NBOUND
#
#USTIME   USBC (for i=1,NSOLUTE)
#       |       |       |
#####
0.000     0.0036
0.033     649.30
0.083     365.00
0.167     667.00
0.250     535.00
0.333     394.00
0.417     542.50
0.500     689.50
0.583     770.00
0.667     792.00
0.750     1052.5
0.833     727.50
0.917     614.00
1.000     582.00
1.083     597.50
1.167     635.00
1.250     847.00
1.333     8.7000
1.417     3.0000
1.500     1.0055
1.583     0.2300
1.667     0.2600
1.750     0.1246
1.833     0.0874
2.000     0.0572
2.167     0.0272
2.500     0.0200
2.883     0.0061

```

Q.inp

```

#####
#####
#
#       OTIS steady flow file
#
# Miller Run - B1 Tracer Study (Fall 2022)
#
#####
#####
0.00      QSTEP [hour]
0.006     QSTART [L^3/second]
#####
#       for I = 1, NREACH

```



```

#
#QLATIN   QLATOUT   AREA   (CLATIN J=1,NSOLUTE)
#   |       |       |       |
#####
5.0e-2   6.0e-2   0.25   0.025
0.00    0.00    0.10   0.025
0.00    0.00    0.10   0.025

```